Geochemistry, Petrogenesis and Alteration of Rare-Metal-Bearing Granitoids and Mineralized Silexite of the Al-Ghurayyah Stock, Arabian Shield, Saudi Arabia

Hisham A. Gahlan [*1], **Mokhles K. Azer**[2], **Paul D. Asimow**[3], **Mansour H. Al-Hashim**[1]

1. *Department of Geology and Geophysics, College of Science, King Saud University, Riyadh* 11451, *Saudi Arabia*
2. *Geological Sciences Department, National Research Centre, Cairo, Egypt*
3. *Division of Geological & Planetary Sciences, California Institute of Technology, Pasadena CA* 91125, *USA*

Hisham A. Gahlan: https://orcid.org/0000-0001-9914-8766

ABSTRACT: New data are presented for the rare-metal bearing A-type granitoids of the Al-Ghurayyah stock in the northwestern segment of the Arabian Shield, a composite pluton intruding metamorphosed volcano-sedimentary successions of the Silasia Formation. Metals in the granitoids are variably enriched, with up to 1 990 μg/g Zn, 7 680 μg/g Zr, 2 316 μg/g Nb, 232 μg/g Ta, 485 μg/g Hf, 670 μg/g Th, 137 μg/g U and 1 647 μg/g total rare earth elements (REE). The silexite is highly mineralized and yields higher maximum concentrations of several metals than the granitoids, including up to 1 860 μg/g Y, 9 400 μg/g Zr, 878 μg/g Hf, 1 000 μg/g Th, and 2 029 μg/g total REE. The Al-Ghurayyah stock has been assigned to an intraplate setting. Lithospheric delamination led to generation of mantle melts that supplied heat to melt the juvenile crust of the ANS. The fluorine and rare-metal enriched parental magma evolved by fractional crystallization. The quartz-rich silexite, distinct in character from ordinary hydrothermal vein quartz, is inferred to be co-genetic with the granitoids on the basis of their similar REE patterns; it is interpreted as a small volume of residual magma enriched in SiO_2, volatiles, and trace metals. Mineralization took place both at the magmatic stage and later during a hydrothermal stage that concentrated these elements to economic grades.

KEY WORDS: Arabian Shield, Al-Ghurayyah, rare metals, silexite, peralkaline granite, hydrothermal metasomatism.

0 INTRODUCTION

A group of elements collectively called rare metals play an increasingly active role in global civilization. The most important rare metals include tantalum, niobium, zirconium, tin, tungsten, titanium, beryllium, and the rare earth elements (REE). These elements are required by numerous strategic industries such as telecommunications, electronics, batteries, and magnets. Geological environments suitable for concentration of these rare metals to economic grades are available in the Arabian Shield, the eastern half of the Arabian-Nubian shield (ANS), which formed by the accretion of intra-oceanic island arcs in the Neoproterozoic upon closing of the Mozambique Ocean (Abdel-Karim et al., 2021; Ali et al., 2010; Stern, 1994) during the Pan-African Orogeny.

The wide distribution of granitoids is one of the most striking features of the Arabian Shield. They were emplaced at various crustal levels with variable ages, tectonic settings, and geochemical characteristics (Abuamarah et al., 2021b; Abdallah et al., 2020; Moghazi et al., 2015; Ali et al., 2014). The period of post-collisional magmatism following assembly of the Shield is marked by the emplacement of numerous alkaline and peralkaline granitoids (Abuamarah et al., 2021a; Moussa et al., 2021; Azer et al., 2010; Stern et al., 2010), many of which are significantly enriched in rare metals (e. g., Gahlan et al., 2022, 2021; Al-Saleh and Al-Omari, 2021; Abdallah et al., 2020; Abuamarah, 2020; Moghazi et al., 2015, 2011). The voluminous post-collisional magmatism of the Arabian Shield represents a significant addition to or reworking of the juvenile crust of the ANS without a nearby plate boundary and hence requires a petrogenetic model beyond conventional plate tectonic processes.

Exploration for rare metals in the Arabian Shield has been continuing for some time (Gahlan et al., 2021; Du Bray, 1986; Ramsay, 1986; Ramsay et al., 1986; Drysdall et al., 1984) and has resulted in the discovery of enrichment in several A-type granitoid plutons and associated pegmatites. Few of these have been assessed in detail for resource potential and, moreover, it remains controversial whether the transportation and enrichment of rare metals in these rocks in primarily a syn-magmatic or a post-magmatic process.

The Al-Ghurayyah stock is thought to be typical in many

---

ways of the rare-metal bearing post-collisional granitoids of the Arabian Shield, but the published record concerning Al-Ghurayyah is sparse and embodies many contradictory interpretations (Johnson et al., 2011; Johnson, 2006; Aleinikoff and Stoeser, 1988; Jackson, 1986). Hence, we selected the Al-Ghurayyah stock as a good opportunity to understand the petrogenetic processes that form mineralized post-collisional granites. This study integrates field work, petrography, mineral chemistry, and whole-rock geochemical analyses as a basis for defining the petrological characteristics, magmatic evolution, and post-magmatic processes that affected the Al-Ghurayyah stock. Our discussion addresses several key questions: (1) whether the Al-Ghurayyah stock represents one or multiple magmatic pulses; (2) how the silexite is related to the host granitoids; (3) to what extent magmatic vs. metasomatic processes were responsible for formation of associated ore deposits; and finally, (4) what implications our results have for the formation and reworking of the juvenile continental crust of the ANS.

1 GEOLOGIC SETTING

The distribution of the most important post-collisional alkaline/peralkaline intrusions in the Arabian Shield is shown in Fig. 1. The Al-Ghurayyah stock is located in the northwest corner of Saudi Arabia, at 27°55′N and 35°48′E. The area lies in the north-central part of the Midyan terrane, a ~50 to 60 km wide strip of Proterozoic basement exposure bordered by Phanerozoic sedimentary cover to the northeast, the coastal plain of the Red Sea to the southwest, the Gulf of Aqaba to the northwest, and the Yanbu suture zone to the southeast. The felsic intrusions in the Midyan region span a range of ages from 725 to 570 Ma (Clark, 1987; Drysdall et al., 1985; Hedge, 1984; Ramsay, 1982).

The study area encompassing the Al-Ghurayyah stock is largely covered by Quaternary sediments (Fig. 2a), with Late Neoproterozoic basement outcrops exposing a metamorphosed volcano-sedimentary succession intruded by a sequence of granitoids. The relationship between the Al-Ghurayyah granite stock and its country rocks, inferred from field observations, is shown in a schematic cross-section (Fig. 2b). The metamorphosed volcano-sedimentary rocks (Silasia Formation) belong to the island-arc stage of crustal evolution in the Arabian Shield. These highly deformed and lineated rocks are the oldest units in the mapped area (>710 Ma; Johnson, 2006) and are intruded by an abundant variety of dikes. The Al-Ghurayyah pluton itself is notably younger: Aleinikoff and Stoeser (1988) obtained a Rb-Sr isochron age of 577 ± 13 Ma and Johnson et al. (2011) concluded that the age of the Al-Ghurayyah pluton is reasonably constrained by the age of the nearby Dabbagh pluton (577 ± 4 Ma by U-Pb in zircon) reported by Hedge (1984).

Outcrops of the Al-Ghurayyah stock together define a broadly circular pluton, dissected by many faults. There is likely to be additional volume of Al-Ghurayyah granitoids underlying much of the alluvial cover. In the field, the discontinuous circular masses of granitoids show marked variation in color, texture, and composition. We divided the Al-Ghurayyah stock itself into quartz syenite, porphyritic granite and peralkaline granite. The contacts between these rock types may be either

sharp or gradational; in weathered areas the subunits and their contacts are difficult to discern. The porphyritic granite intrudes the quartz syenite (Fig. 2c), while peralkaline granite intrudes porphyritic granite (Fig. 2d). No xenoliths were observed and the sparsity of mafic dikes cutting the granitoids stands in marked contrast to the numerous dikes in the metamorphosed volcano-sedimentary country rocks. Some parts of the stock show marginal tectonic brecciation and pervasive cataclasis.

Quartz syenite is recorded only in the northern mass as a few outcrops of reddish to pinkish color (Fig. 3a). Porphyritic granite is the most common rock type in the stock; it was previously labeled alkali feldspar granite by Elliott et al. (1999). It is fine- to medium-grained and porphyritic with whitish to pinkish color (Fig. 3b). Peralkaline granite is rare and only observed at the margins of the southernmost outcrop. It is fine- to medium-grained, light grey (Fig. 3c), and contains a few miarolitic cavities. Along the contact with peralkaline granite, the porphyritic granite shows variable degrees of alteration including silicification, sericitization, chloritization and hematization (marked by red color where iron-rich mafic minerals have been oxidized).

Several dikes, pods and veins of pegmatite, fluorite, quartz, and silexite crosscut the margins of the stock. Pegmatite occurs as pockets or veins, concentrated at the southern margins of the stock. It consists of very coarse crystals of K-feldspars and quartz (Fig. 3d). Fluorite in marginal veins and pods shows various colors ranging from violet to blue and green (Fig. 3e). Non-mineralized, monomineralic white quartz veins (<0.30 m wide) are uncommon; they are associated with fluorite veins along fault planes. Silexite occurs as veins (0.20–0.60 m wide) and segregated masses (<0.5 m in all dimensions). Texturally, these fine-grained veins could also be named aplite, but we prefer silexite because of their quartz-dominant mineralogy (there is some debate over whether "silexite" as an igneous rock name should be replaced by "quartzolite", since "silexite" refers to sedimentary chert in French; however, we prefer the classical term "silexite" for highly quartz-rich igneous rocks). Silexite has sharp and sheared contacts with the surrounding granites. In hand-specimen, silexite may be dark brown (Fig. 3f), mottled yellowish-brown (Fig. 3g), or occasionally zoned with whitish-gray cores and brown rims (Fig. 3h).

2 PETROGRAPHY

Here we offer petrographic descriptions of each rock type (quartz syenite, porphyritic granite, peralkaline granite, and silexite), confirming the field identification.

2.1 Quartz Syenite

As noted above, quartz syenite is a minor rock type, outcropping only in the northern area of the stock. It is an inequigranular medium-grained rock and rarely shows porphyritic texture. K-feldspars and albite are the essential minerals with minor quartz and mafic minerals. Accessory minerals include zircon, columbite, allanite, pyrochlore, muscovite, apatite and Fe-Ti oxides. Albite occurs as subhedral prismatic crystals, partly or completely altered to sericite and muscovite (Figs. 4a, 4b). K-feldspars include both orthoclase and microcline. Micro-
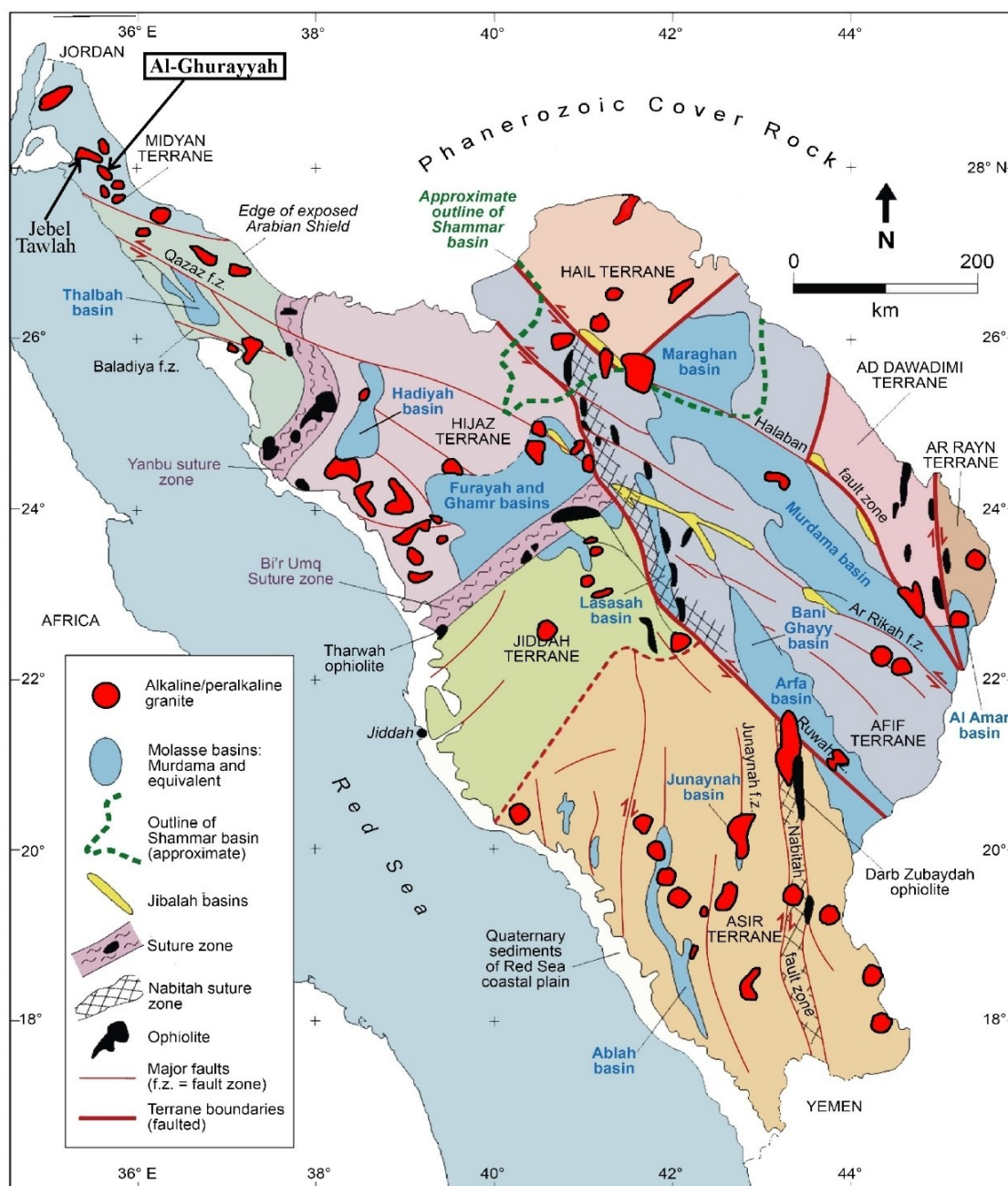
Figure 1. Simplified geologic map of the Arabian Shield in Saudi Arabia (modified after Stern and Johnson, 2010), indicating the distribution of major features such as suture zones, basins, ophiolites, faults, and terrane boundaries. The distribution of alkaline/peralkaline granites and ring complexes are shown in red. The location of the Al-Ghurayyah intrusion is indicated.

cline is partly replaced by secondary albite. Quartz occurs as anhedral granular crystals showing undulose extinction and containing a few feldspar inclusions. The main mafic mineral is sodic amphibole containing inclusions of K-feldspars, zircon and apatite (Fig. 4c).

Subhedral to anhedral zircon crystals have a dark brown to reddish color; both primary and secondary zircons are present in the quartz syenite. The primary zircon is inclusion-free and features oscillatory zoning. Secondary zircon contains sparse inclusions. Its zoning is patchy or absent, it is commonly associated with columbite and rutile, and it commonly has xenotime overgrowths. Some anhedral crystals of Nb-Ta oxides, especial-

ly columbite, are observed in the quartz syenite. Pyrochlore forms yellow to reddish-yellow subhedral crystals, mostly associated with sodic amphibole and Nb-Ta oxides (Fig. 4d). Allanite occurs as pleochroic reddish-brown anhedral crystals (Fig. 4e). Muscovite occurs as anhedral interstitial crystals (Fig. 4f). Fe-Ti oxides occur as granular aggregates associated with altered mafic minerals. Apatite occurs as fine needles.

2.2   Porphyritic Granite

Porphyritic granite is fine- to medium-grained with porphyritic texture. It consists essentially of phenocrysts of quartz, albite, and K-feldspars set in a fine-grained groundmass. The
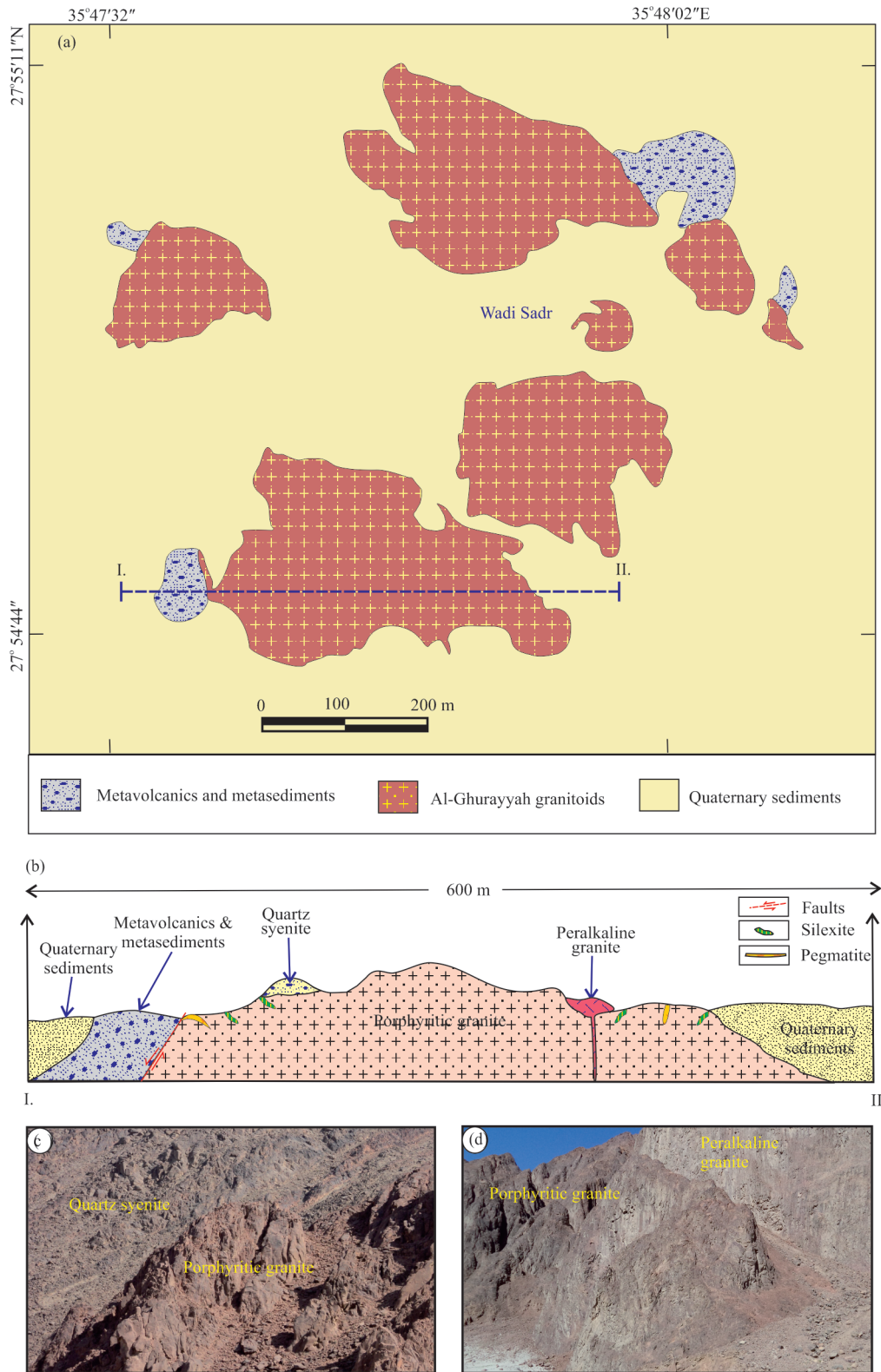
Figure 2. (a) Geologic map of the Al-Ghurayyah area, modified after Elliott et al. (1999); (b) general geological cross section showing the relation between the Al-Ghurayyah stock and its country rocks; (c) field photograph showing the porphyritic granite intruding the quartz syenite, width of field of view is 10 m; (d) field photograph of the peralkaline granite intruding porphyritic granite, width of field of view is 15 m.

groundmass is dominantly quartz, albite and K-feldspars with scarce micas and skeletal crystals of amphibole. The accessory minerals include zircon, fluorite, monazite, columbite-tantalite, thorite, cassiterite, and xenotime. Albite is the dominant mineral (30 vol% – 40 vol%) and forms subhedral prismatic phenocrysts containing zircon inclusions (Fig. 5a) as well as fine lath-shaped crystals that make up 70%–80% of the groundmass and form an intergranular texture with fine-grained quartz. Over-

Figure 3. Hand specimen photographs of the studied rocks: (a) quartz syenite, (b) porphyritic granite, (c) peralkaline granite, (d) pegmatite, (e) fluorite, (f) dark-brown silexite, (g) yellowish-brown silexite, and (h) whitish-gray zoned silexite.

growths of secondary albite are observed around primary feldspars and quartz. Some albite phenocrysts have been partially altered to sericite and muscovite. Quartz (20%–30%) occurs as anhedral to subhedral large phenocrysts (10–15 mm) showing undulose extinction or as very fine anhedral crystals in the groundmass. There are also veins and fine aggregates of quartz filling cavities. Many inclusions of albite, zircon, pyrochlore, and mica occur in the large quartz phenocrysts (Fig. 5b). A few

large quartz crystals contain abundant inclusions of albite, oriented parallel to the host crystal faces, forming a snowball texture (Fig. 5c). K-feldspars (15%–20%) are mainly microcline, which forms subhedral to anhedral phenocrysts (5–10 mm) displaying cross-hatched twinning as well as fine-grained crystals in the groundmass. A few large microcline phenocrysts are partly converted to pseudomorphs of secondary albite (Fig. 5d).

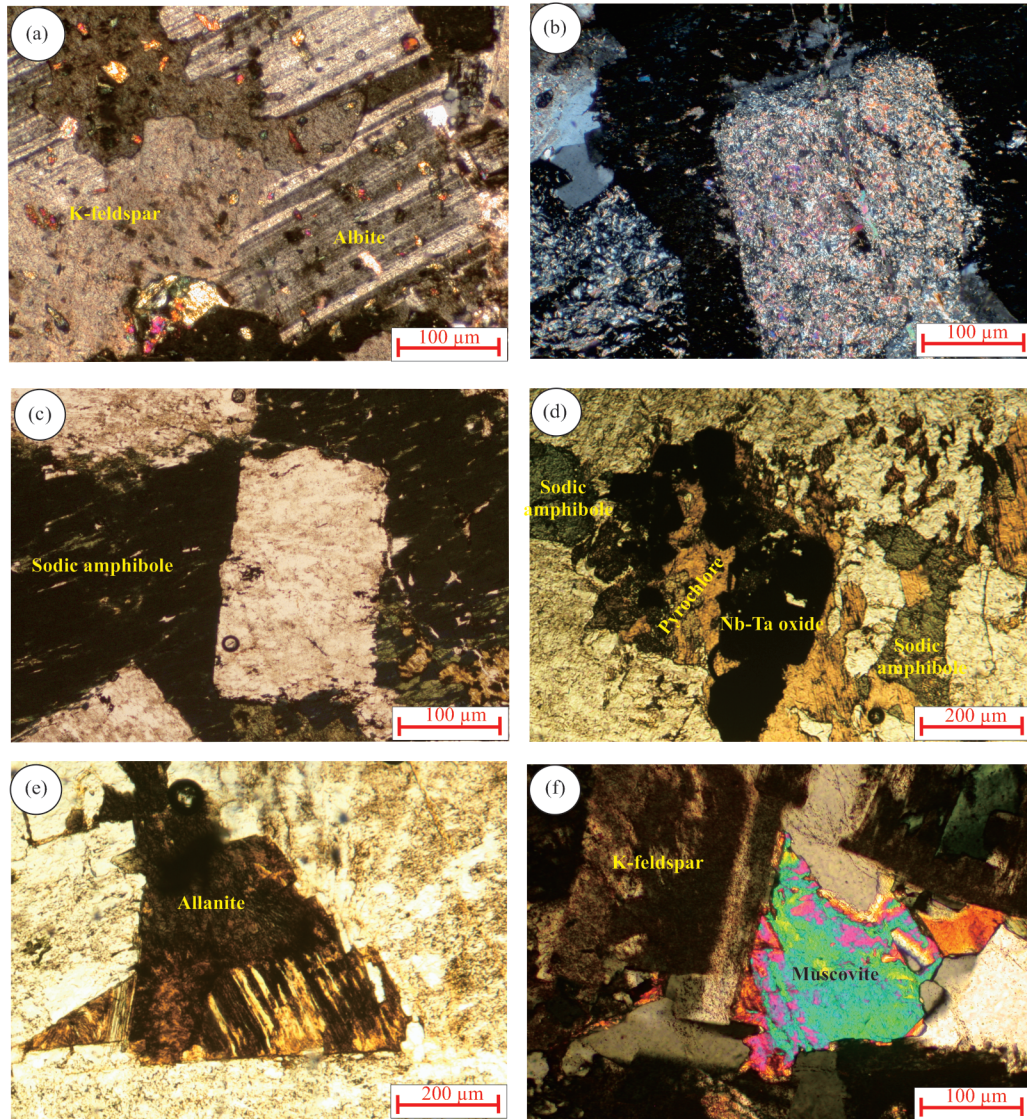Micas occur as inclusions in quartz and K-feldspar pheno-

Figure 4. Petrographic features in quartz syenite. Panels (a), (c), (d) and (e) in plane-polarized transmitted light; (b) and (f) in cross-polarized transmitted light. (a) Prismatic crystals of albite partly altered to sericite and muscovite, (b) feldspar crystals completely altered to sericite and muscovite, (c) sodic amphibole containing euhedral crystal of K-feldspar, (d) pyrochlore associated with sodic amphibole and Nb-Ta oxides, (e) anhedral crystals of allanite, and (f) muscovite interstitial to feldspars.

crysts or as microphenocrysts in the groundmass (Fig. 5e). Zircon is the most common accessory mineral in the porphyritic granite. It occurs as disseminated crystals in the groundmass or as inclusions in the quartz and K-feldspar phenocrysts. Subhedral to anhedral primary zircon is common as inclusions in the phenocrysts; it is clear to light brown, inclusion-free, and shows oscillatory zoning (Fig. 5f). Secondary zircon is darker and reddish; it occurs as patches or rims around primary zircon, with a characteristic spongy texture (Putnis, 2009). Secondary zircon is locally associated with hematite, rutile, chlorite and muscovite. Columbite occurs as anhedral to subhedral crystals disseminated among other minerals; no variations in columbite color are apparent under the microscope.

2.3 Peralkaline Granite

Peralkaline granite occurs at the margins of the Al-Ghurayyah stock. It is a fine- to medium-grained rock and rare-

ly shows porphyritic texture. It consists essentially of K-feldspars, quartz, albite and sodic amphibole with rare sodic pyroxene. Accessory minerals include zircon, fluorite, micas, columbite-tantalite, thorite, xenotime, pyrochlore, bastnaesite, fergusonite and samarskite. K-feldspars (30% – 35%) occur as subhedral to anhedral crystals of perthitic orthoclase and cross-hatch twinned microcline (Fig. 6a). Quartz (20% – 30%) occurs as anhedral to subhedral crystals or as inclusions in the alkali feldspars; some large quartz phenocrysts display a snowball texture due to aligned albite inclusions. Albite (10% – 15%) occurs as lath-shaped crystals included in the quartz and K-feldspar phenocrysts. Sodic amphibole (3% – 7%) occurs as subhedral crystals (up to 5 mm) with strong dark blue to green pleochroism (Fig. 6b) and as acicular interstitial crystals. Microprobe analyses (see below) show that the sodic amphiboles are riebeckite and arfvedsonite. Sodic amphibole may be partially altered to chlorite and opaques. Aegirine occurs as rims around
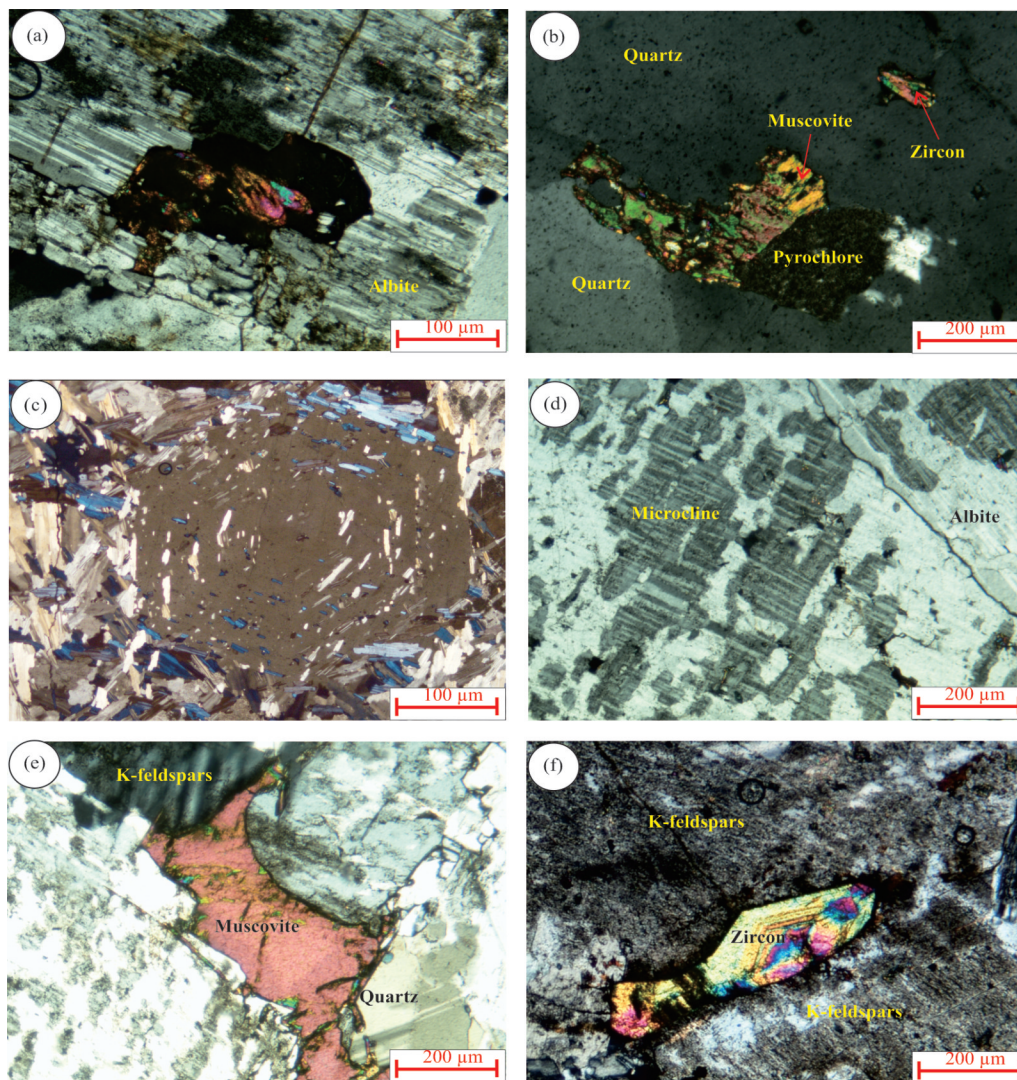
Figure 5. Petrographic features in porphyritic granite (all photos are taken in cross-polarized transmitted light): (a) albite phenocryst containing zircon inclusion, (b) inclusions of zircon, pyrochlore and muscovite in quartz phenocryst, (c) snowball texture of albite laths arranged concentrically in quartz, (d) microcline phenocryst partially replaced by albite with preservation of the original twinning, (e) anhedral interstitial muscovite crystal, and (f) zoned crystal of zircon.

sodic amphibole and as acicular fine crystals.

Zircon is present as inclusions in sodic amphibole (Fig. 6c) and as disseminated, subhedral, dark brown to dark yellow prismatic crystals closely associated with pyrochlore. Columbite is the most common Ta-Nb oxide, occurring in various forms associated mainly with sodic amphibole and micas (Fig. 6d). A few columbite crystals exhibit color variation suggestive of compositional zoning. Subhedral to euhedral fresh crystals of mica in the peralkaline granite include muscovite (Fig. 6e) and polylithionite-siderophyllite solid solution (i. e., zinnwaldite) (Fig. 6f) with rare biotite. Fergusonite occurs as dark brown anhedral crystals, altered to pyrochlore at the rims (Fig. 6g). Pyrochlore also forms rounded yellowish-brown grains (Fig. 6h). Fluorite occurs as anhedral to subhedral interstitial grains and as small veins. Bastnaesite and samarskite occur as anhedral small crystals associated with pyrochlore.

2.4   Silexite

Silexite occurs as siliceous veins that, in hand specimen,

may appear pinkish, dark-brown, or reddish-brown. These colors may be mottled together or zoned across the vein. Silexite samples are fine-grained and display a cataclastic fabric. They are composed of anhedral quartz (65% – 80%), K-feldspars, sodic amphibole, aegirine, micas, hematite, and ore minerals. Quartz shows variable grain size that ranges from <100 μm up to 1.5 cm. The large quartz crystals are cracked and contain many vapor-rich fluid inclusions. Also, veinlets of secondary quartz are observed cutting the other minerals. K-feldspars occur as large turbid crystals, stained with iron oxide and partly to completely altered to sericite. Sparse microcline crystals preserve cross-hatch twinning. Sodic amphibole occurs as separated crystals (Fig. 7a) or as irregular clumps (Fig. 7b). The margins of separated amphibole crystals are replaced by chlorite. Aegirine occurs as subhedral small crystals, partly altered to hematite. Micas include zinnwaldite, muscovite and rare biotite. Zinnwaldite forms large subhedral fractured crystals, partly altered to chlorite.

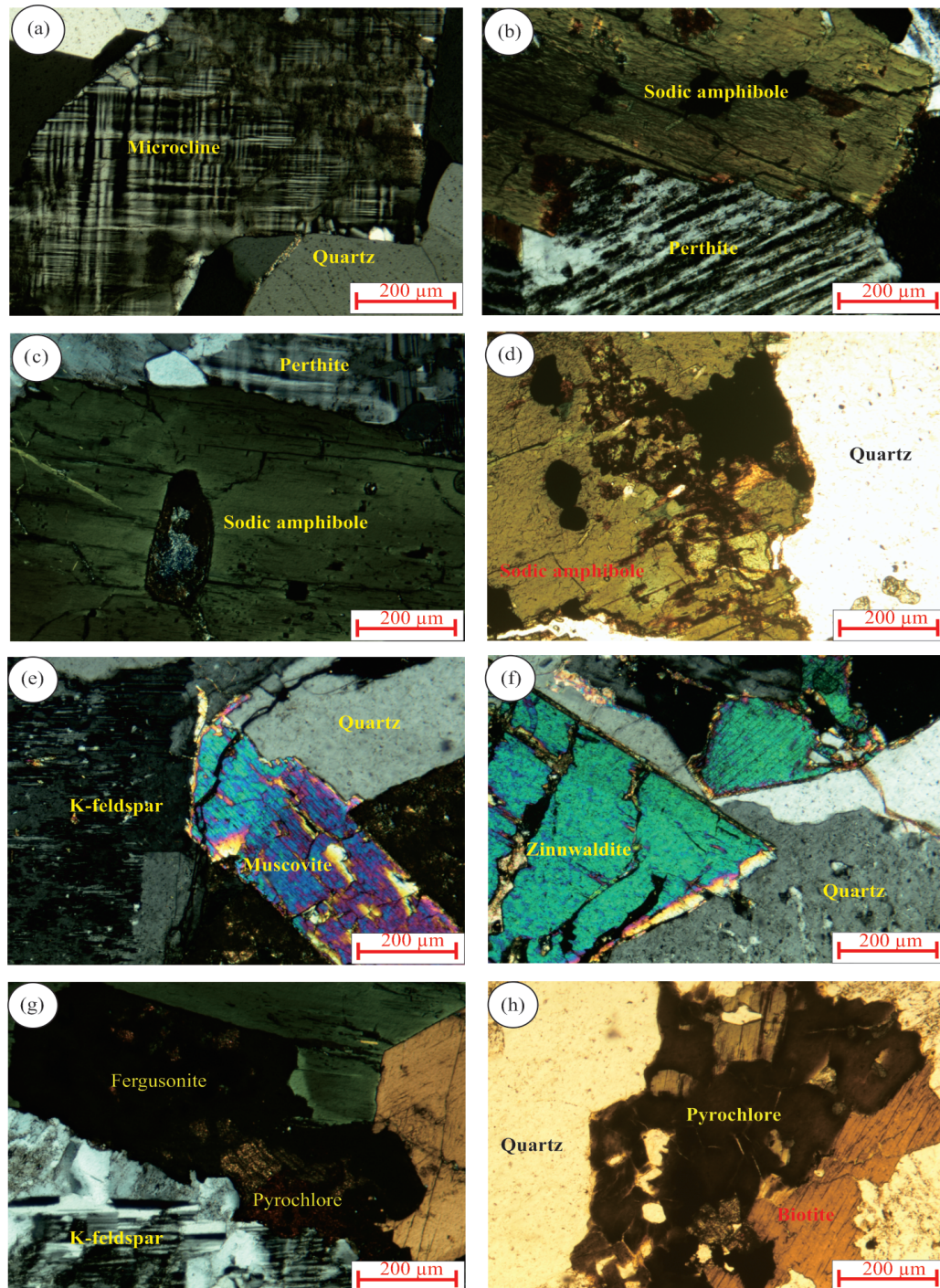Ore minerals occur in silexite as aggregates (Fig. 7c) that

Figure 6. Petrographic features in peralkaline granite. Panels (d) and (h) in plane-polarized transmitted light; (a), (b), (c), (e), (f) in cross-polarized transmitted light: (a) microcline showing cross-hatch twinning, (b) corroded tabular crystal of sodic amphibole, (c) zircon inclusion in sodic amphibole, (d) Nb-Ta oxides associated with sodic amphibole, (e) muscovite crystal interstitial to K-feldspar and quartz, (f) cracked zinnwaldite crystal, (g) fergusonite crystal altered at the margins to pyrochlore, and (h) anhedral crystals of pyrochlore associated with biotite.

may include zircon, columbite, allanite, pyrochlore, xenotime, thorite, monazite, cassiterite, rutile and REE minerals (bastnaesite, fergusonite and samarskite). Zircon is the most common ore-mineral, forming subhedral to anhedral scattered crystals from 50 to 400 µm long. Zircon varies in color from reddish-brown to colorless; reddish-brown zircons are rich in inclusions of thorite and hematite. Columbite and pyrochlore are the main Nb minerals. Columbite occurs as subhedral prismatic crystals (100–600 µm long) that contain inclusions of zircon. Scarce light yellow anhedral disseminated crystals (<100 µm long) are identified as pyrochlore, replaced at the margins by thorite. Cassiterite occurs as fine aggregates; as small, rounded crystals with intense brown color; and as small irregular inclusions (<5 µm) in rutile. Monazite occurs as fine disseminated grains and fracture filling. Xenotime occurs as interstitial grains or as overgrowths on zircon.
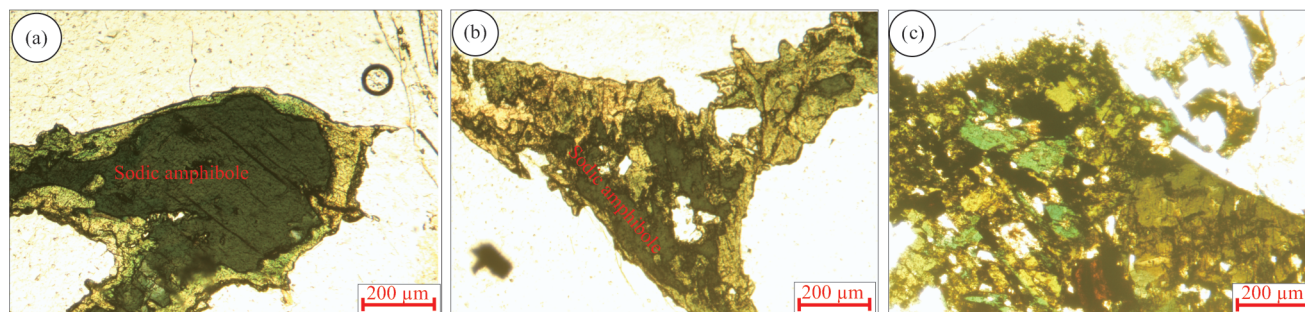
Figure 7. Petrographic features in silexite (all photos in plane-polarized transmitted light): (a) large sodic amphibole crystal altered along its margins into chlorite, (b) irregular clumps of sodic amphibole, and (c) ore mineral aggregates.

3   ANALYTICAL TECHNIQUES

Representative polished thin sections were prepared and carbon-coated for microprobe analyses. Mineral compositions were obtained using a CAMECA SX100 electron probe (EPMA) at the Department of Geosciences (University of Oslo). The EPMA was operated with a 15 kV, 15 nA, 2 μm diameter beam, for 10 s counting time on-peak and 5 s each at low and high background positions. Synthetic oxide and mineral standards and a ZAF matrix correction routine were used. The standards were all accepted international standards and included natural albite for Na and Al; natural orthoclase for K; synthetic anorthite for Ca; natural zircon for Zr and Si; synthetic rutile for Ti; synthetic fayalite for Fe; synthetic forsterite for Mg; natural fluorapatite for P; and pure metals for Mn, Nb, Sn, Hf, and Ta. Kα X-rays were used for all elements except Zr (Lα), Nb (Lα), Sn (Lα), Hf (Mα), and Ta (Mα). X-rays with energies between 1.0 and 1.8 keV were analyzed with TAP crystals, between 1.8 and 5.0 keV with PET crystals, and above 5.0 keV with LIF crystals.

Based on the petrographic investigations, 28 representative samples covering the different rock types of the Al-Ghurayyah stock were selected for bulk chemistry analysis (major, trace and rare earth elements). The analyzed samples were crushed and pulverized to ~40 mesh using an agate mortar and agate ring mill and then quartered several times to obtain representative samples. Major element compositions and concentrations of Sc, Ba and Ni were determined by inductively coupled plasma-atomic emission spectrometry (ICP-AES). The remaining trace elements and the rare earth elements (REE) were determined by inductively coupled plasma-mass spectrometry (ICP-MS). Loss on ignition (LOI) was determined by weight difference after ignition at 1 000 ºC. The bulk chemistry analyses were carried out at the Activation Laboratories Ltd (Actlabs), Ontario, Canada. Analytical precision, as calculated from replicate analyses, is 1% for major elements, 2%–10% for trace elements, and 0.5%–3% for REE.

4   RESULTS
4.1   Mineral Chemistry

The identification of the essential and accessory minerals under the microscope was refined and supported by EPMA, however, a number of accessory minerals (allanite, pyrochlore, monazite, thorite, xenotime, bastnaesite, fergusonite and samarskite) were not suitable for microprobe analysis due to their small size and the limited number of elements that can be analyzed in a practical protocol. The complete mineral chemistry

dataset is given in the Electronic Appendix (Supplementary Tables S1 to S14).

4.1.1   Silicate minerals

The analyzed silicate minerals include mafic minerals (amphiboles, aegirine and micas), feldspars, zircon and chlorite.

4.1.1.1   Mafic minerals

The analyzed mafic minerals in the Al-Ghurayyah stock include aegirine, amphiboles and micas. Aegirine crystals, though rare, were located and analyzed in peralkaline granite and silexite. The chemical compositions and structural formulae based on 6 oxygens of the analyzed aegirine are given in supplementary Table S1. The analyses have low apparent probe totals when assuming total Fe as FeO; recalculated totals after assignment of Fe^{3+} in the structural formula are acceptable.

Amphiboles were analyzed in quartz syenite, peralkaline granite and silexite. The chemical composition and structural formulae based on 22 non-W-site oxygens are listed in supplementary Table S2. According to the classification scheme of Hawthorne et al. (2012), the amphibole analyses range from sodic-calcic to sodic. Sodic-calcic amphibole is found in quartz syenite and ranges across varieties of winchite, hastingsite, richterite and katophorite. Sodic amphibole is found in peralkaline granite and silexite and includes both magnesio-arfvedsonite and riebeckite.

The analyzed micas include (presumed) muscovite and annite. We have not analyzed the micas for Li, F, or Fe^{3+} content and therefore the assignment of the aluminous trioctahedral mica observed here to muscovite is preliminary; it may in fact correspond to the material optically identified as zinnwaldite. Muscovite occurs in quartz syenite, porphyritic granite, peralkaline granite and silexite, whereas annite is found only in silexite. Supplementary Table S3 gives chemical compositions and structural formulae (on the basis of 11 oxygens) of the analyzed micas. Petrographically primary muscovite was analyzed in peralkaline granite and silexite, whereas petrographically secondary muscovite was analyzed in quartz syenite, porphyritic granite and peralkaline granite. Secondary muscovite has lower TiO_2 and higher MgO than primary muscovite. On the Ti-Mg-Na ternary discrimination diagram after Miller et al. (1981), the petrographically primary muscovite plots as expected in the primary field, whereas the secondary muscovite plots in the secondary field (Fig. 8a). Annite in silexite is not plotted because this discrimination diagram does not apply to this mineral.

4.1.1.2   Feldspars

Feldspars were analyzed in all main rock phases of the Al-Ghurayyah stock; they include K-feldspars and albite. The chemical compositions and structural formulae on the basis of 8 oxygen atoms are given in supplementary Table S4 (K-feldspar) and Table S5 (albite). K-feldspars are homogenous, nearly pure $KAlSi_3O_8$, with K_2O content ranging from 14.4 wt.% to 16.3 wt.% and Or content ranging from 95.3 mol% to 98.4 mol%.

Albite is the only plagioclase mineral in the Al-Ghurayyah granites. It has Na_2O content ranging from 11.0 wt.% to 11.8 wt.%. It is almost pure end-member albite (95.2 mol% to 99.0 mol%), with a small variation in An content between 0.0 mol% and 2.3 mol%. The presence of distinct K-feldspar and albite coexisting with occasional perthite grains in all granite phases of the stock suggests crystallization under subsolvus conditions followed by minor exsolution (Abuamarah et al., 2022).

4.1.1.3   Zircon

Zircon was analyzed in all main phases of the Al-Ghurayyah stock and is close to chemically pure $(Zr, Hf)SiO_4$. Both primary and secondary zircons were analyzed in quartz syenite, porphyritic granite and peralkaline granite. The compositions and calculated structural formulae of the analyzed zircons are given in supplementary Table S6. Most of the analyzed secondary zircons yield somewhat low electron probe analytical totals (92.3 wt.%–95.7 wt.%), likely due to the metamict character of these Neoproterozoic, highly radioactive, zircons. The primary zircon is richer in SiO_2 (31.6 wt.%–32.4 wt.%) and ZrO_2 (59.9 wt.%–61.5 wt.%) but lower in MnO (0.14 wt.%–0.34 wt.%) and HfO_2 (3.0 wt.%–4.4 wt.%) than secondary zircon (27.6 wt.%–29.9 wt.% SiO_2, 48.8 wt.%–55.4 wt.% ZrO_2, 0.74 wt.%–3.4 wt.% MnO and 5.4 wt.%–11.2 wt.% HfO_2).

4.1.1.4   Chlorite

The analyzed chlorite is an alteration product after amphiboles and sodic pyroxene. The chemical composition and structural formulae on the basis of 28 oxygens of chlorite from quartz syenite and peralkaline granite are given in supplementary Table S7. They are classified mainly as ripidolite with minor brunsvigite.

4.1.2   Non-silicate minerals

The analyzed non-silicate minerals include Nb-Ta oxides, cassiterite, Fe-Ti oxides and apatite.

4.1.2.1   Nb-Ta minerals

Chemical analyses and structural formulae of columbite and tantalite are given in supplementary Table S8. Columbite is the main primary Nb-Ta bearing phase in all rock types of the Al-Ghurayyah stock, while tantalite is a secondary phase and is found only in quartz syenite and porphyritic granite. The major oxides in both columbite and tantalite are Nb_2O_5, Ta_2O_5, MnO, and FeO. The apparent SiO_2 in tantalite is likely due to imperfect correction for the interference of the X-ray lines of Si and Ta. Columbite has Mn/(Mn+Fe) ratios from 0.64 to 0.85 and Ta/(Nb+Ta) ratios from 0.07 to 0.40; it is classified as columbite-(Mn) (Fig. 8b). The analyzed tantalite occurs as well-defined overgrowths or replacement mantles around primary columbite. Tantalite has Ta/(Nb+Ta) ratios from 0.53 to 0.63 and Mn/(Mn+Fe) ratios from 0.61 to 0.87, it is classified as tantalite-(Mn) (Fig. 8b).

4.1.2.2   Cassiterite

Cassiterite is analyzed in the porphyritic granite and silexite and the results are given in supplementary Table S9. The apparent concentration of CaO in cassiterite is an artifact of an uncorrected interference between the $K\alpha$ line of Ca and the $L\beta_1$ line of Sn. The only oxide other than SnO_2 that appears to be robustly detected in cassiterite is ~0.9 wt.% SiO_2. Although, when analyzing fine cassiterite crystals, there is a risk of counting Si X-rays from secondary fluorescence in adjacent silicates, the consistent value obtained (independent of grain size or neighboring phase identity) suggests that the Si is in fact hosted in the cassiterite lattice or in homogeneously distributed nano-inclusions.
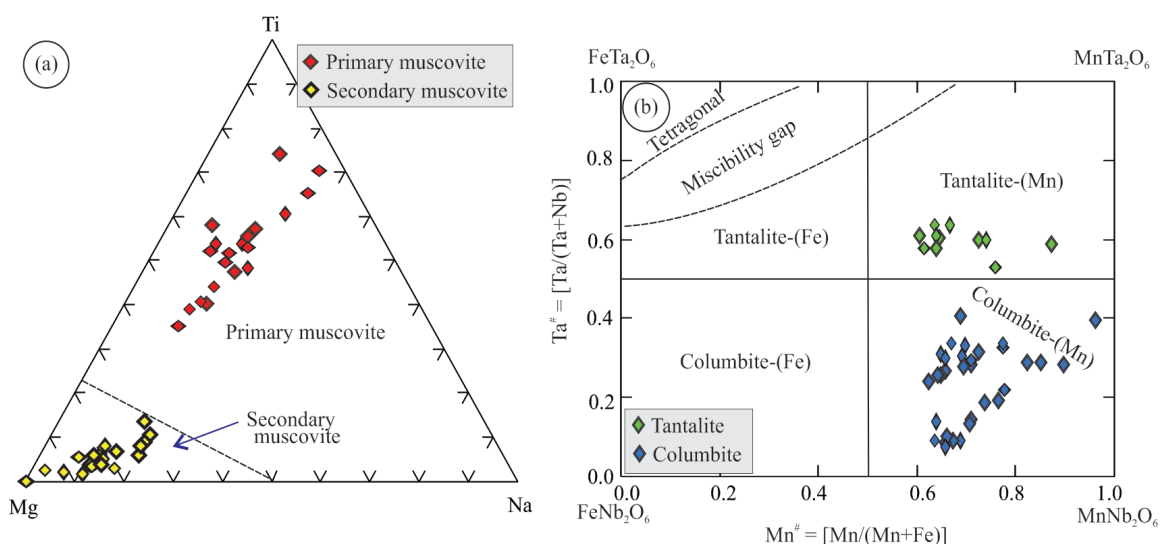

Figure 8. Mineral chemistry of the Al-Ghurayyah stock. (a) Mg-Ti-Na ternary diagram with compositional fields of primary and secondary muscovite after (Miller et al., 1981). (b) Chemical composition and nomenclature of the columbite-tantalite group minerals based on Ta/(Ta+Nb) *vs*. Mn/(Mn+Fe) ratios.

4.1.2.3   Fe-Ti oxides

The analyzed Fe-Ti oxides include magnetite, ülvospinel, ilmenite, rutile and goethite. Analyses of spinel-group Fe-Ti oxides (magnetite-ülvospinel solid solutions) are given in supplementary Table S10 with 4-oxygen calculated structural formulae and mineral names assigned by the 50% rule. All analyses in quartz syenite and porphyritic granite are magnetite, with Ti atoms per formula unit (apfu) lower than Fe^{3+} apfu. However, while all magnetite analyses in porphyritic granite have $TiO_2 \leqslant 0.7$ wt.% (Ti apfu $\leqslant 0.02$), the quartz syenite also contains a population of titanomagnetite with up to 6.8 wt.% TiO_2 (Ti apfu up to 0.21). The peralkaline granite contains both low-Ti magnetite ($TiO_2 \leqslant 1.0$ wt.%) and a population of very high-Ti grains straddling the boundary between titanomagnetite and ülvospinel (15.7 wt.%–27.6 wt.% TiO_2 and Ti apfu 0.46–0.80).

Ilmenite was analyzed in quartz syenite and peralkaline granite; compositions and calculated structural formulae based on 3 oxygens are given in supplementary Table S11. Significant substitution of Mn for Fe^{2+} is observed, with MnO varying from 1.0 wt.% up to 19.8 wt.%. Pyrophanite (end member Mn-TiO_3) component is a common substitution for ilmenite in oxidized granitic rocks (Deer et al., 1992).

Goethite is a common alteration mineral in all rock types at Al-Ghurayyah. Microprobe analyses of goethite-rich aggregates are given in supplementary Table S12. The analyses of goethite have low totals because it is a hydrous, porous phase and is likely intermixed at nano-scale with other minerals. FeO* is the main constituent (61.4 wt.%–76.5 wt.%), alongside variable amounts of SiO_2 (3.8 wt.%–9.5 wt.%) and TiO_2 (0.9 wt.%–3.0 wt.%).

Rutile is a common accessory mineral in the peralkaline granite and silexite; microprobe analyses of rutile are given in supplementary Table S13. The analyzed rutile is nearly pure TiO_2 (93.3 wt.%–98.9 wt.%) with the main substituent being FeO* (0.8 wt.%–3.6 wt.%).

4.1.2.4   Apatite

Apatite was observed in quartz syenite and peralkaline granite. Partial microprobe analyses for apatite are given in supplementary Table S14; the analyses have low totals because fluorine and chlorine were not analyzed. The analyses cannot be assigned to a particular apatite-group mineral species with

these data. CaO (45.0 wt.%–48.6 wt.%) and P_2O_5 (35.6 wt.%–40.1 wt.%) are the major detected oxides, with smaller but non-negligible amounts of Na_2O (0.9 wt.%–2.4 wt.%). Na substitution in apatite is often associated with carbonate ion substitution, but C was not analyzed.

4.2   Whole Rock Major and Trace Element Composition

Only limited geochemical data on the Al-Ghurayyah granitoids has been published to date (Drysdall and Douch, 1986). Whole-rock analyses (major oxides, trace elements and rare earth elements) of the granite and silexite samples are listed in Tables S15, S16 and S17. All the samples are felsic, with high SiO_2, Al_2O_3 and total alkali (K_2O+Na_2O) contents and low TiO_2, Fe_2O_3, MgO, MnO, CaO and P_2O_5 contents. The samples are all Na-rich, with Na_2O/K_2O ratios from 1.2 to 8.0. On the R_1-R_2 diagram (where $R_1 = 4Si - 11(Na + K) - 2(Fe + Ti)$ and $R_2 = 6Ca + 2Mg + Al$; De la Roche et al., 1980), the samples petrographically assigned to quartz syenite plot as expected in the quartz syenite field, whereas the porphyritic and peralkaline granite sample plot in the alkali granite field (Fig. 9a). The major oxide and trace element contents of the granitoids show mostly smooth variations as functions of silica content on Harker variation diagrams (Figs. 10, 11): K_2O increases with increasing SiO_2, while TiO_2, Al_2O_3, MgO, MnO, CaO and Na_2O decrease with increasing SiO_2 (Fig. 10). Fe_2O_3* and P_2O_5 are essentially uncorrelated with SiO_2. Trace element data show progressive enrichment of Rb, Y, Ta, Nb, Th and Ga alongside depletion of Sr and Ba with increasing SiO_2 (Fig. 10). The remaining trace elements are not significantly correlated with SiO_2.

The granitoid compositions yield agpaitic index values [AI = (Na+K)/Al on a molar basis] greater than 0.87 (0.93–1.23, Table S15), indicating alkaline/peralkaline character (Liégeois et al., 1998; Liégeois and Black, 1987). On the Shand's index diagram, A/NK versus A/CNK (Fig. 9b), the samples lie mainly in the peralkaline field with a few samples extending into the metaluminous field. The alkaline/peralkaline character of the bulk chemistry is consistent with the presence of modal aegirine and sodic amphibole and of normative acmite (0.61–1.25; Table S16). The discrimination diagram of Sylvester (1989) (Fig. 9c) places the granitoids mostly in the alkaline field, with a few extending into the highly-fractionated field where calc-alkaline and alkaline suites overlap. The granitoid
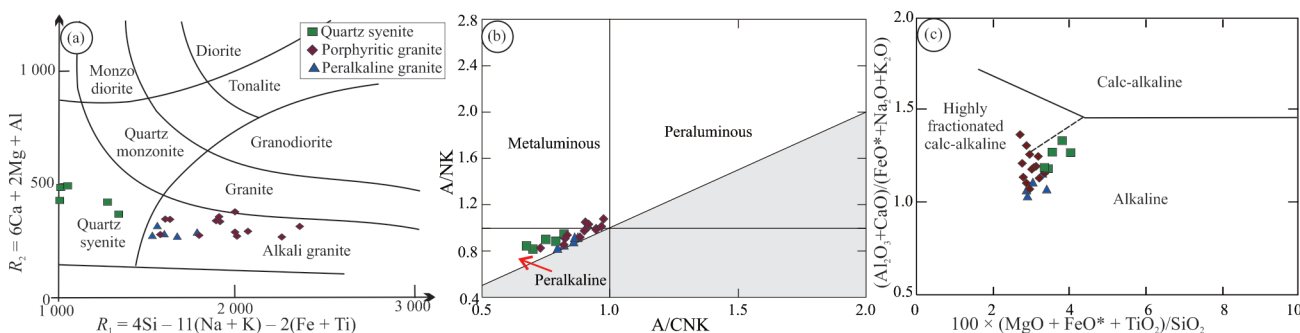

Figure 9. Discrimination diagrams based on whole-rock chemistry. (a) Nomenclature of Al-Ghurayyah granitoids using the R_1-R_2 diagram of de la Roche et al. (1980). Note legend for three granitoid varieties of the Al-Ghurayyah stock. (b) Shand's index plot, molar $Al_2O_3/(Na_2O+K_2O)$ versus $Al_2O_3/(CaO +Na_2O+K_2O)$ (after Maniar and Piccoli, 1989). (c) $100\times(MgO+FeO*+TiO_2)/SiO_2$ vs. $(Al_2O_3+CaO)/(FeO*+Na_2O+K_2O)$, with fields of calc-alkaline, highly fractionated calc-alkaline, and alkaline granites (Sylvester, 1989).
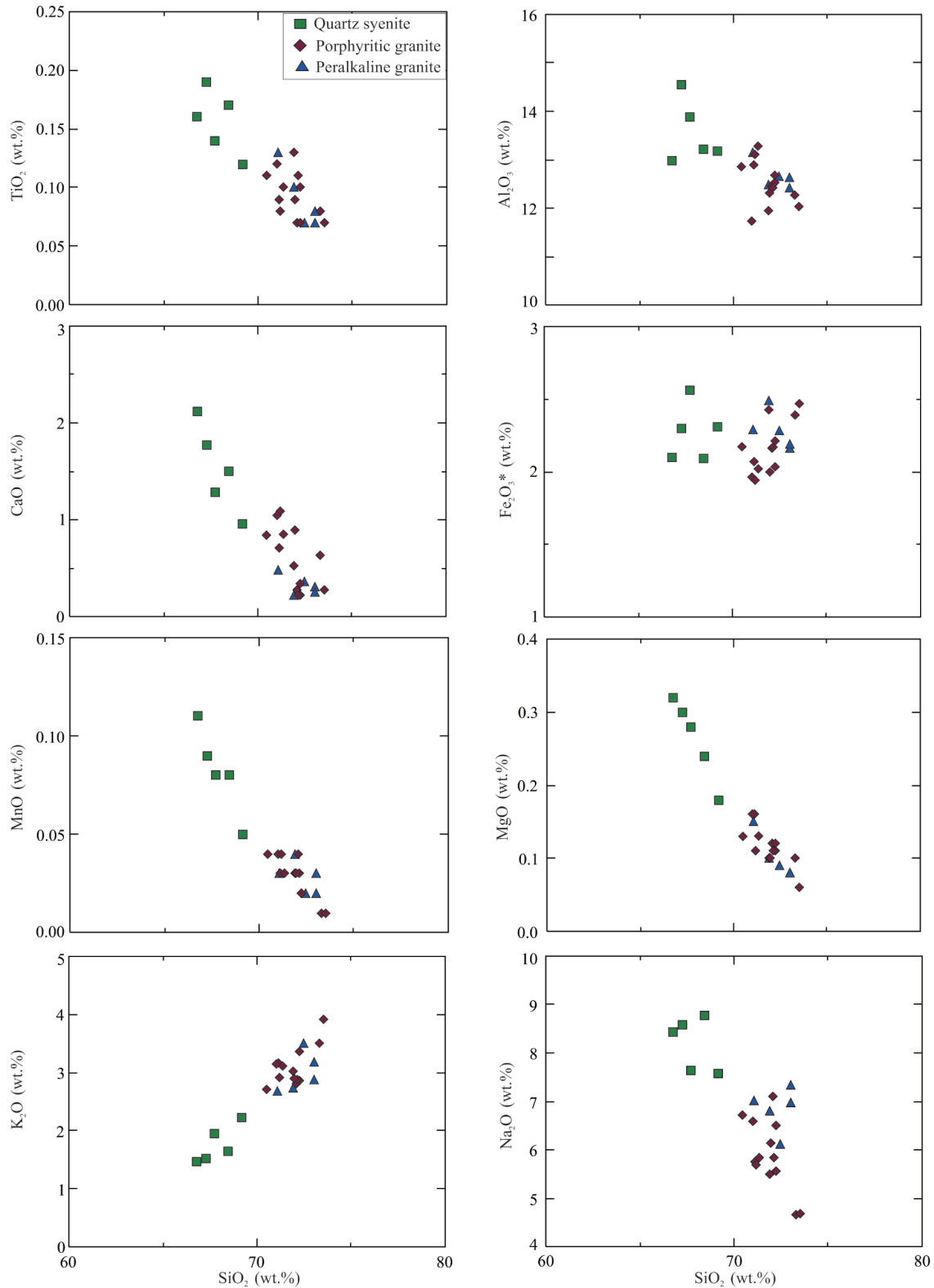
Figure 10. Variation diagrams of some major oxides against SiO_2.

samples share all the characteristics of A-type granites, such as high Nb, Y, Ta, Hf, Th, Zr and Ga/Al, alongside significant depletion in MgO, CaO and P_2O_5 (Bonin, 2007; Eby, 1992, 1990; Whalen et al., 1987).

On the Ga/Al $vs.$ FeO_t/MgO diagram of Whalen et al. (1987), Al-Ghurayyah granites plot in the A-type field (Fig. 12a). The typical A-type character of Al-Ghurayyah granites is supported by using the SiO_2 $vs.$ FeO_t/(FeO_t+MgO) discrimination diagram of Frost et al. (2001), on which the samples plot as typical ferroan A-type granites (Fig. 12b). Plotting the Al-Ghurayyah granitoid data on the discrimination diagrams of Eby (1992) reveals that they are similar to the A_1 subgroup
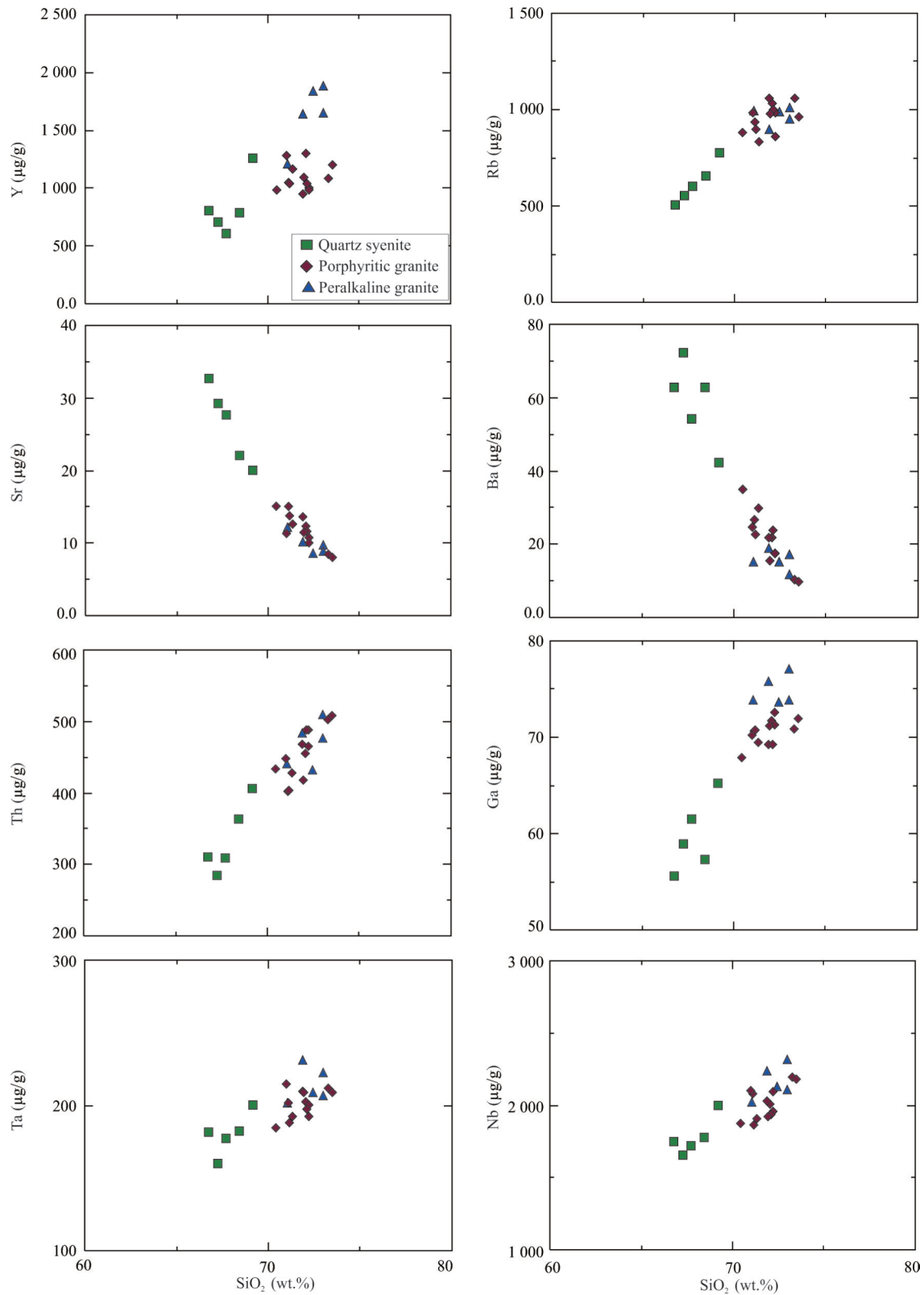
Figure 11. Variation diagrams of some trace elements against SiO₂.

(Figs. 12c, 12d), like mineralized African A-type granites such as the Ririwai and Gross Spitzkoppe suites (Vonopartis et al., 2021).

Primitive mantle-normalized multi-element patterns, using normalization values of Sun and McDonough (1989), of each

variety of Al-Ghurayyah granitoids and silexite are shown in Fig. 13. All samples of the three granitoid varieties display nearly uniform patterns marked by large enrichments in some large-ion lithophile elements (Rb, Th, U, Pb) and high field strength elements (Ta, Nb, Zr, Hf) alongside clear depletions in
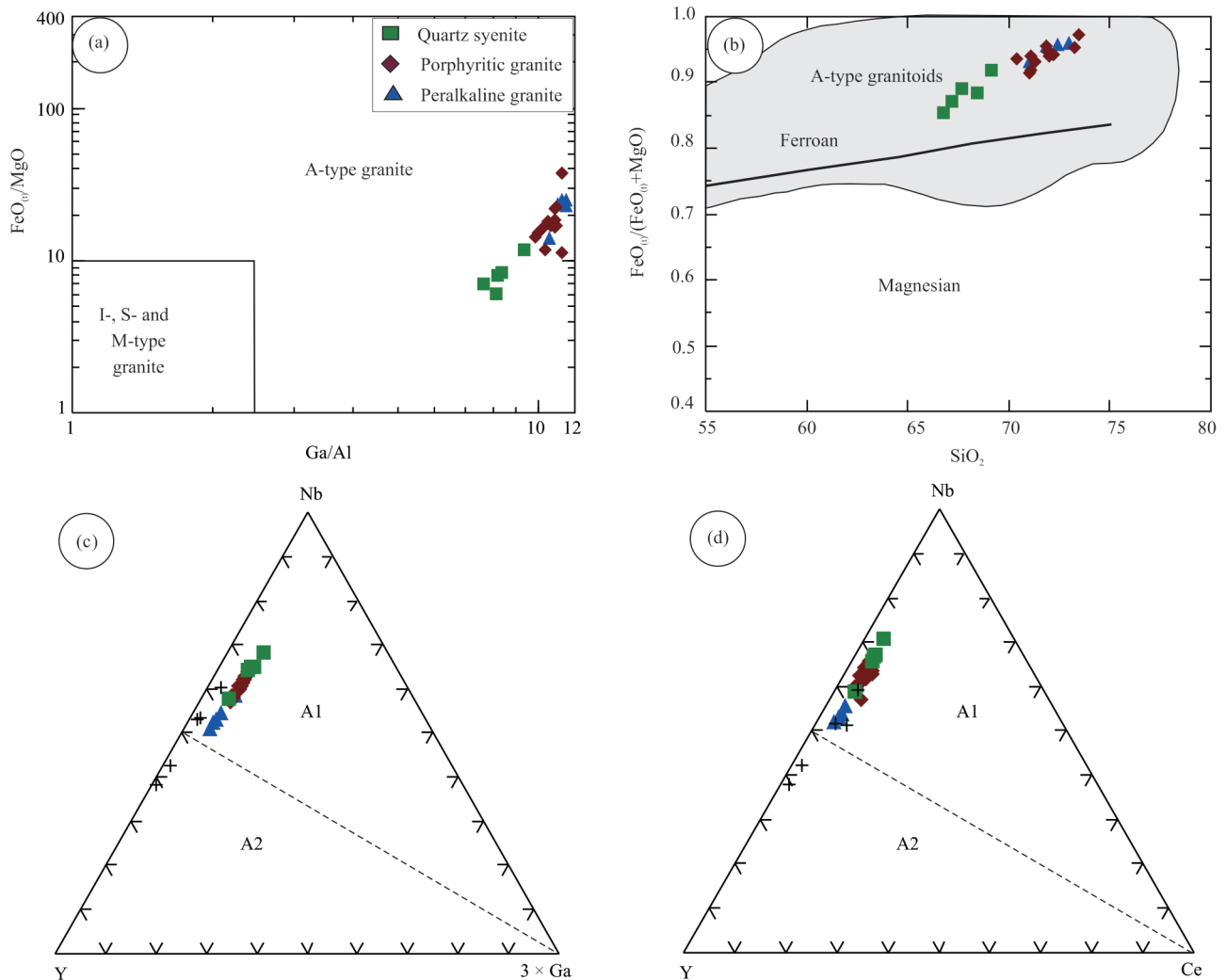
Figure 12. Additional discrimination diagrams for granitoid types. (a) Ga/Al *vs*. FeO$_{(t)}$/MgO (Whalen et al, 1987), (b) SiO$_2$ *vs*. FeO$_{(t)}$/(FeO$_{(t)}$+MgO) diagram (Frost et al., 2001), (c) Nb-Y-Ga×3 ternary diagram (Eby, 1992), and (d) Nb-Y-Ce ternary diagram (Eby, 1992).

Ba, Sr, P, Eu and Ti. Concentrations of Nb-Ta are not anomalous compared to neighboring elements. The silexite samples show patterns quite similar to the granites except for about an order of magnitude higher P concentrations (Fig. 13d).

Chondrite-normalized REE patterns (using the chondrite values of Evensen et al., 1978) are presented in Fig. 14. The quartz syenite samples have lower total REE contents (533–717 μg/g) than the porphyritic granite (759–1 403 μg/g), peralkaline granite (882–1 647 μg/g) and silexite (887–2 029 μg/g). All samples display notable enrichment in heavy REE (HREE) relative to light REE [(La/Lu)$_n$ = 0.01 – 0.29]. The REE patterns of quartz syenite and porphyritic granite are subparallel with uniformly positive HREE slopes, while the peralkaline granite samples have striking concave-down HREE patterns. The magnitude of HREE enrichment is notably larger in the silexite samples than in the granitoids. Strongly negative Eu anomalies [(Eu/Eu*) = 0.05 – 0.11] are present in all rock types. Alongside the two order-of-magnitude negative anomalies in Sr and Ba, this indicates an extended history of plagioclase fractionation earlier in the petrogenetic history than represented by any of the exposed samples, under conditions reducing enough to stabilize some Eu^{2+}. Residual plagioclase in the

source would not be able to generate negative anomalies as large as those observed from a source with initially flat Sr, Ba, and Eu patterns (McKay, 1989; Hanson, 1978).

5   DISCUSSION
5.1   Tectonic Setting and Geodynamic Implications

The optimal way to identify the tectonic environment of the Al-Ghurayyah stock is to consider all the available information from field relationships, petrography, mineralogy, and geochemistry. This integrated approach reduces the risk of misassignment that can result from the use of geochemical data alone. Field investigations demonstrate that the stock was emplaced during a non-orogenic period, after the termination of deformation associated with the Pan-African orogeny. Regionally, this stage is characterized by a dramatic transition in the character of magmatism, from typical subduction-related calc-alkaline compositions via late-orogenic calc-alkaline rocks to post-collisional alkaline/peralkaline suites. The alkaline magmatism is usually related to major extension-related structural trends and represents a period of transition from orogenic activity to intra-plate stable conditions (Azer et al., 2021).

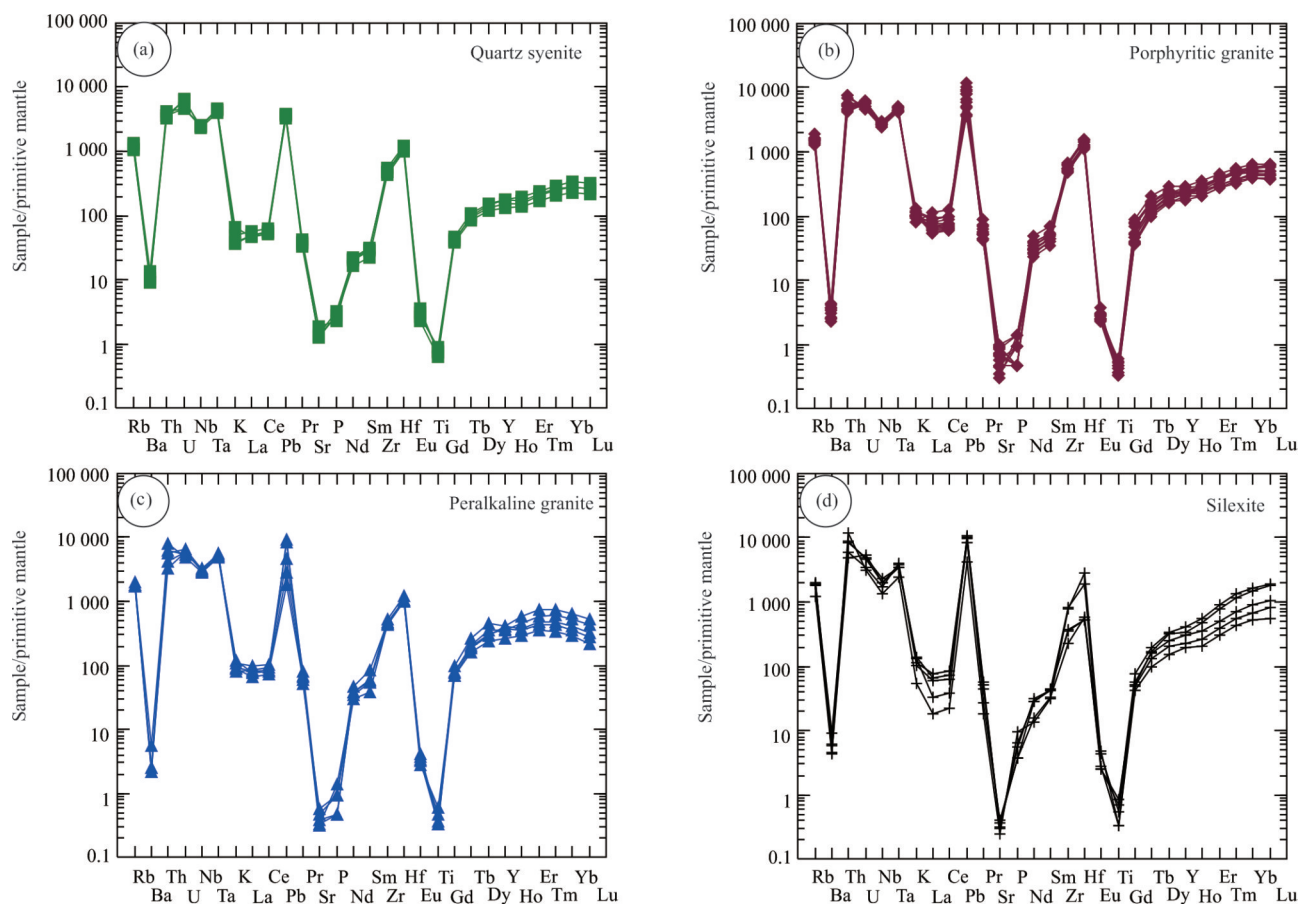The overall chemical characteristics of the Al-Ghurayyah

Figure 13. Primitive mantle-normalized multi-trace element diagrams for whole-rock chemistry of the Al-Ghurayyah stock using normalization values from Sun and McDonough (1989). (a) Quartz syenite, (b) porphyritic granite, (c) peralkaline granite, and (d) silexite.

stock are consistent with a within-plate tectonic setting. They show remarkable depletion in CaO, MgO, Sr and transition metals alongside high alkali contents and marked enrichment in HFSE and REE. The REE patterns contain pronounced negative Eu anomalies. These geochemical features are each typical of within-plate magmatism (Eby, 1992, 1990; Whalen et al., 1987). The within-plate tectonic setting of the Al-Ghurayyah stock is substantiated by plotting the geochemical data on suitable discrimination diagrams. On the SiO_2-Al_2O_3 diagram of Maniar and Piccoli (1989) (Fig. 15a), the analyzed granite samples plot within the rift-related and post-orogenic granite fields. Using the R_1-R_2 tectonic setting discrimination diagram of de la Roche et al. (1980), with tectonic setting fields based on Batchelor and Bowden (1985), the Al-Ghurayyah granitoid samples plot in the anorogenic and post-orogenic fields (Fig. 15b). On the Rb/30-Hf-3 × Ta ternary diagram of Harris et al. (1986), all the granite samples plot far into the within-plate field (Fig. 15c).

We interpret the Al-Ghurayyah stock to be a product of partial melting of a juvenile crustal source, followed by extensive fractional crystallization. The generation of crustal melts parental to Al-Ghurayyah and other similar A-type post-collisional plutons, widely distributed in the ANS, was likely facilitated by a combination of elevation of the crustal geotherm (due to input of mantle-derived heat) and exhumation of the deep crust to low pressure (due to erosion of overburden re-

sulting from uplift). Ascent of the resulting melts to the upper crust, where they underwent extensive fractionation, was in turn likely facilitated by large-scale intra-continental strike-slip fault systems and shear zones that accommodated an extensional tectonic environment. A lithospheric delamination model is commonly invoked to explain the coincidence of these features (crustal heating, doming and erosion, extensional tectonics) with magmatism in the post-collisional stage (610 – 590 Ma) of the Arabian Shield (Abuamarah et al., 2021b; Abdallah et al., 2020).

The proposed model for the tectono-magmatic evolution of Al-Ghurayyah stock through the partial melting of the juvenile crust of the Arabian Shield during the post-collisional phase is shown in Fig. 15d. In this model, crustal and lithospheric thickening during the collisional stage of the Arabian Shield was followed by slab break-off and lithospheric delamination. Delamination forced upwelling of hot asthenosphere, which resulted in broad crustal doming and uplift of the overlying crust. Decompression of asthenosphere generated mafic magma that would have ponded at the base of the crust and efficiently delivered sensible and latent heat to the lower crust. At deeper crustal levels, the combination of anomalously elevated temperature and decompression can cause partial melting. Storage and fractionation of the resulting crustal melts in the middle crust allow the evolution of A-type granites. The abundance of strike-slip faults and shear zones during the post-
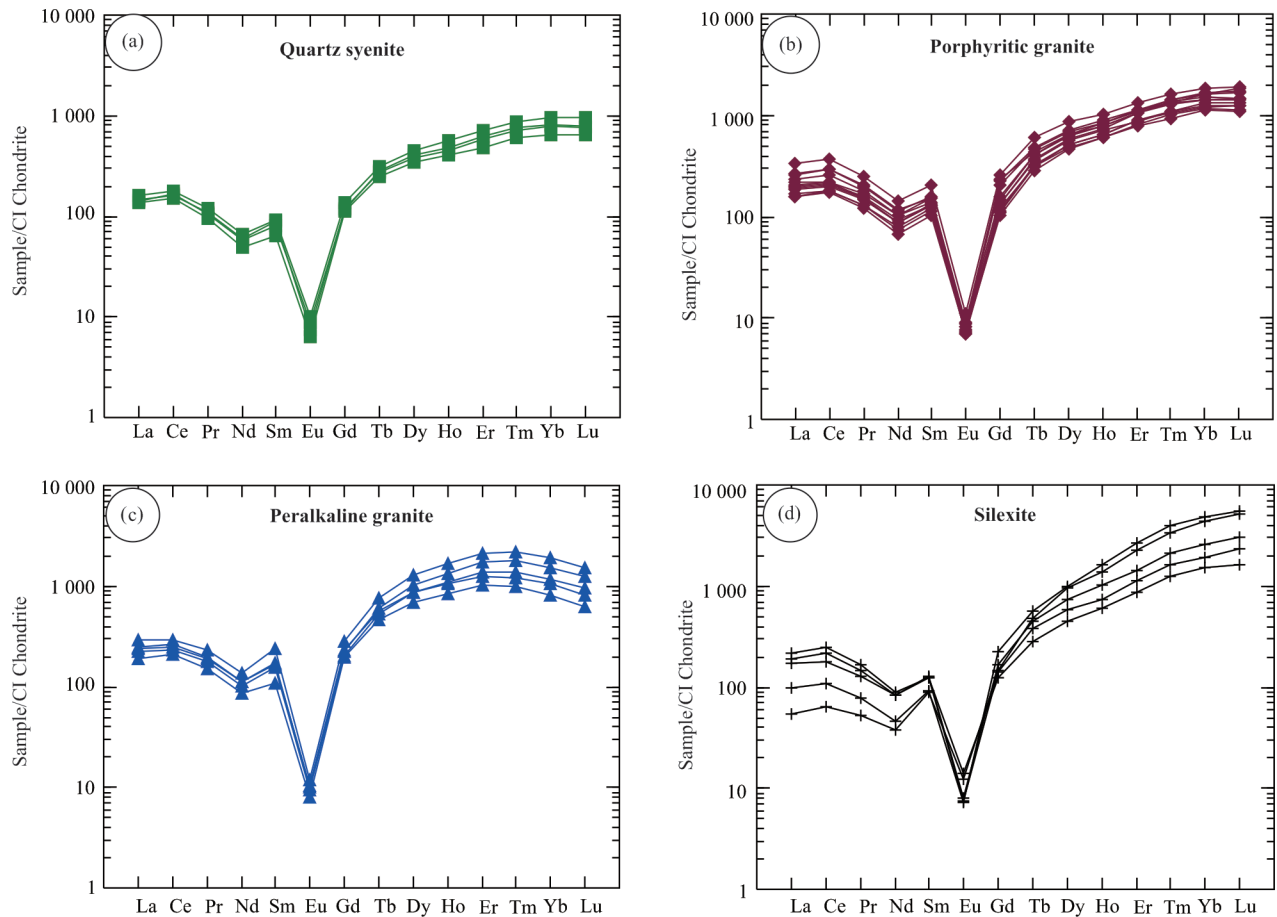
Figure 14. Chondrite-normalized REE patterns for Al-Ghurayyah samples using chondrite values from Evensen et al. (1978). (a) Quartz syenite, (b) porphyritic granite, (c) peralkaline granite, and (d) silexite.

collisional stage promotes the ascent of these magmas to the shallow crust, explaining their common alignment along these structural trends. The Al-Ghurayyah stock, located among a network major faults and shear zones, is evidently a prime example of this mechanism (Elliott et al., 1999; Drysdall and Douch, 1986).

5.2   Source Rocks and Petrogenesis

The present data indicate that the Al-Ghurayyah stock has geochemical features typical of rare-metal bearing A-type granites and was emplaced in the post-collisional period, the final stage of magmatic evolution of the Arabian Shield. Several potential sources and petrogenetic models have been proposed for such intrusions (Abuamarah et al., 2021b; Al-Saleh and Al-Omari, 2021; Gahlan et al., 2021; Abdallah et al., 2020; Moghazi et al., 2015; Ali et al., 2014). However, this category includes rock suites spanning a wide range of major and trace element concentrations and isotope ratios, suggesting that a variety of sources and processes were involved in their genesis. Hence, we may not simply choose one of the previously proposed models; we must consider the data in further detail.

The Al-Ghurayyah stock is marked by clear intrusive contacts against its metamorphic country rocks but gradational boundaries among its different petrologic types. Moreover, all the Al-Ghurayyah granitoid samples have remarkably similar normalized trace element (Fig. 13) and REE (Fig. 14) patterns

and display continuous evolutionary trends in major and trace element concentrations (Figs. 11, 12) and ratios of compatible and incompatible elements (Fig. 16). These lines of evidence suggest that the stock is a well-defined distinct plutonic body and that all its granitoid members evolved from a common parental magma, mostly through fractional crystallization processes. The magmatic evolution is consistent with the sequence of intrusion, with the quartz syenite emplaced before the more evolved porphyritic granite and peralkaline granite.

We judge it unlikely that this parental magma was a mantle-derived mafic liquid. There are no enclaves, xenoliths, or associated mafic igneous rocks that might point to a mafic parent. Indeed, the generation of highly evolved A-type granite by continuous fractional crystallization of a mafic parent is quite inefficient; it would have required at least nine times the volume of the final product in initial mafic magma (Winter, 2014, 2001; Farahat and Azer, 2011; Turner et al., 1992). Nevertheless, generation of the parental magma of the Al-Ghurayyah granites may be linked to mantle processes, specifically to a lithospheric delamination event that triggered upwelling of asthenospheric mantle material beneath the ANS (see 6.5. Geodynamic implications). The upwelling that follows lithospheric delamination allows generation of mantle melts that would be expected to ascend to the density contrast at the base of the ANS crust, supplying a source of heat whose conduction upwards can drive crustal melting. Moreover, the isostatic and dynamic conse-
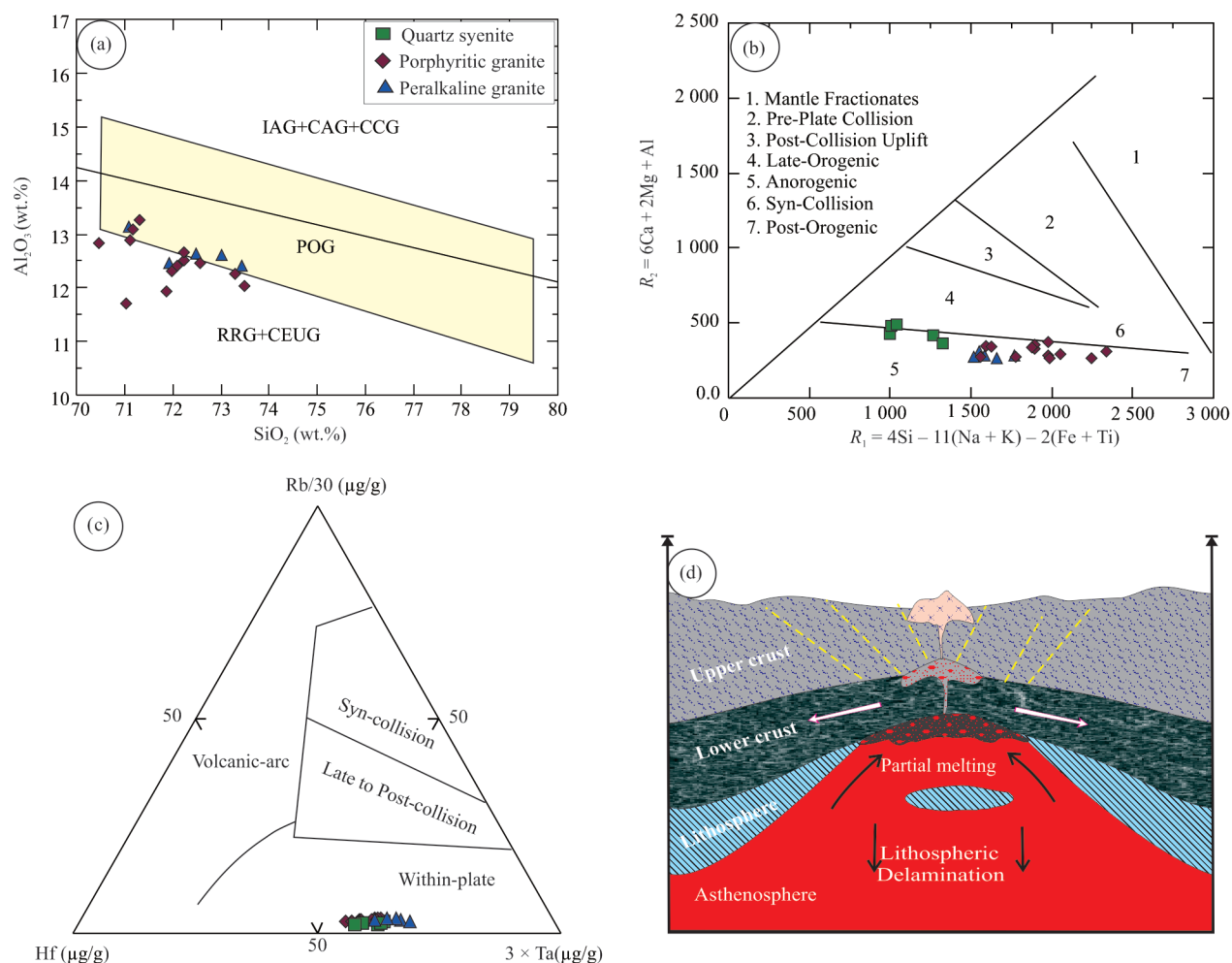
Figure 15. Discrimination diagrams for tectonic setting based on whole-rock chemistry. (a) SiO_2 *vs.* Al_2O_3 after Maniar and Piccoli (1989); (b) R_1-R_2 multicationic diagram (Batchelor and Bowden, 1985); (c) Hf-Rb/30-3×Ta ternary diagram (after Harris et al., 1986); (d) simplified model for the geodynamic evolution of Al-Ghurayyah stock showing how lithospheric delamination triggered upwelling of asthenospheric mantle, generation of underplated basic magma, doming upwards, partial melting of lower and middle crust, generation of A-type granitic magma, ascent and emplacement of fractionated magma extending to subvolcanic levels, and finally erosional removal of cover to expose the top of the pluton.

quence of delamination is an episode of rapid crustal uplift recorded by unroofing of the subduction- and collision-related rocks and development of intersecting strike-slip faults and shear zones.

In this scenario, clearly both mantle-derived and crust-derived melts would have been present at depth. Geochemical criteria must be used to distinguish their relative contributions to the parental magma of the Al-Ghurayyah intrusion. Although Nd isotope ratios are often used to distinguish mantle-derived from ancient crustal sources for magmatic systems, this approach does not work well in the ANS, where potential crustal sources for post-collisional magmatism were themselves quite juvenile at the time and had not yet ingrown distinctively crustal Nd isotope signatures (e.g., Eyal et al., 2010). Hence, we turn to other lines of evidence to test for the presence of mantle-derived contributions to the source of the Al-Ghurayyah parental magma.

Nb/Ta ratios (9.2 – 10.4) in the Al-Ghurayyah granites overlap with typical crustal values (8 – 14; Stepanov and Hermann, 2013) but are clearly lower than the chondritic ratio

(19.9 ± 0.6; Münker et al., 2003) or those observed in many ocean island basalts (15.9 ± 0.6; Pfänder et al., 2007). Likewise, Zr/Hf ratios (15.1 – 16.6) in the Al-Ghurayyah granites plot in the range associated with crustal sources (Zr/Hf < 25; Wedepohl, 1995). As discussed below, these crustal signatures are present in all rocks of the suite and show no increase with progressive differentiation, suggesting they are a signature of the primary magma and not of later assimilation during magmatic evolution. The contribution of the juvenile crust of the Arabian Shield to the Al-Ghurayyah stock is also demonstrated by the presence of inherited zircons with ages of 749.9 ± 5.9 Ma (Aseri, 2020). This conclusion is substantiated by plotting the data on the ternary discrimination diagram of Laurent et al. (2014), which suggests that the Al-Ghurayyah granites were derived from Low-K mafic rocks and tonalitic sources, which are indeed the main constituent of the early subduction-related magmatic rocks of the ANS with ages near 750 Ma (Fig. 17a).

Field relations indicate that the quartz syenite, restricted to the northern margin of the outcrop, is the preserved remnant of the apex of a magma chamber, exposing a shallow level of
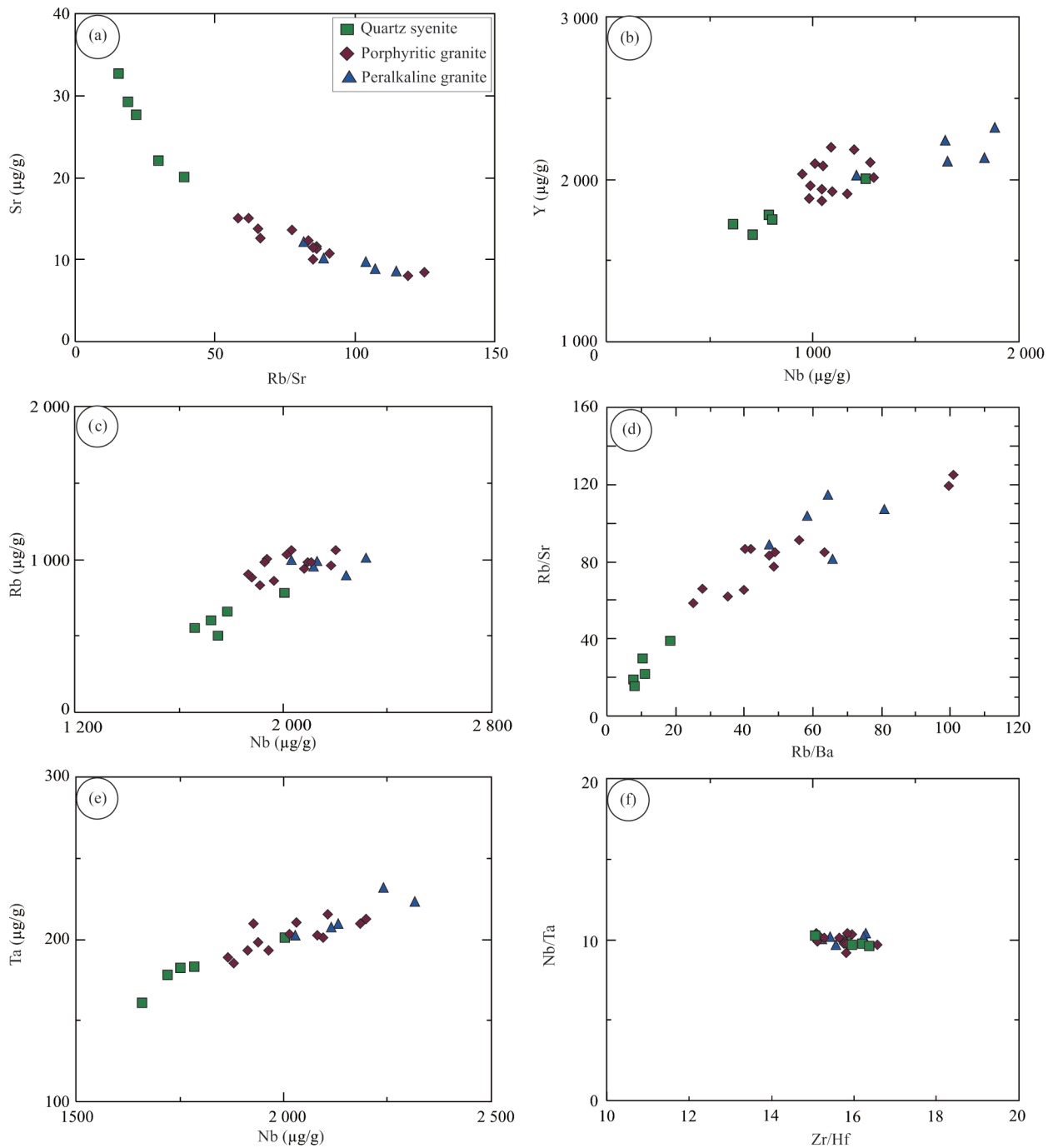
Figure 16. Some trace element diagrams indicating magmatic evolution of the Al-Ghurayyah granitoid series: (a) Sr *vs.* Rb/Sr, (b) Y *vs.* Nb, (c) Rb *vs.* Nb, (d) Rb/Sr *vs.* Rb/Ba, (e) Ta *vs.* Nb, and (f) Nb/Ta *vs.* Zr/Hf.

emplacement. It is likely that the main mass of the stock resembles the porphyritic granite that composes the bulk of the outcrop. The peralkaline granite, a minor phase in the southern portion of the outcrop area, is likely a later phase intruded into the porphyritic granite while the latter was still hot and fluid. The gradational contacts between different phases in the stock indicate their emplacement within a very short time interval, before the complete crystallization of the first porphyritic phase (though sharp contacts are also observed, suggesting that the rigidity of early phases was variable from place to place when intruded by later phases). During the final peralkaline

stage, the residual melt became enriched in alkalis, silica, water, and fluorine and must have achieved fluid saturation (it may have already been fluid saturated at earlier stages) (London, 1992). The buoyancy and low viscosity of the F- and water-rich melt and vapor phases promoted their migration to the top of the magma chamber and into fractures extending into the earlier magmatic phases and the country rocks of the intrusion. They are preserved as pegmatite, silexite and quartz-fluorite veins.

The occurrence of magmatic fluorite and F-rich secondary Nb-Ta minerals indicate appreciable enrichment of the mag-
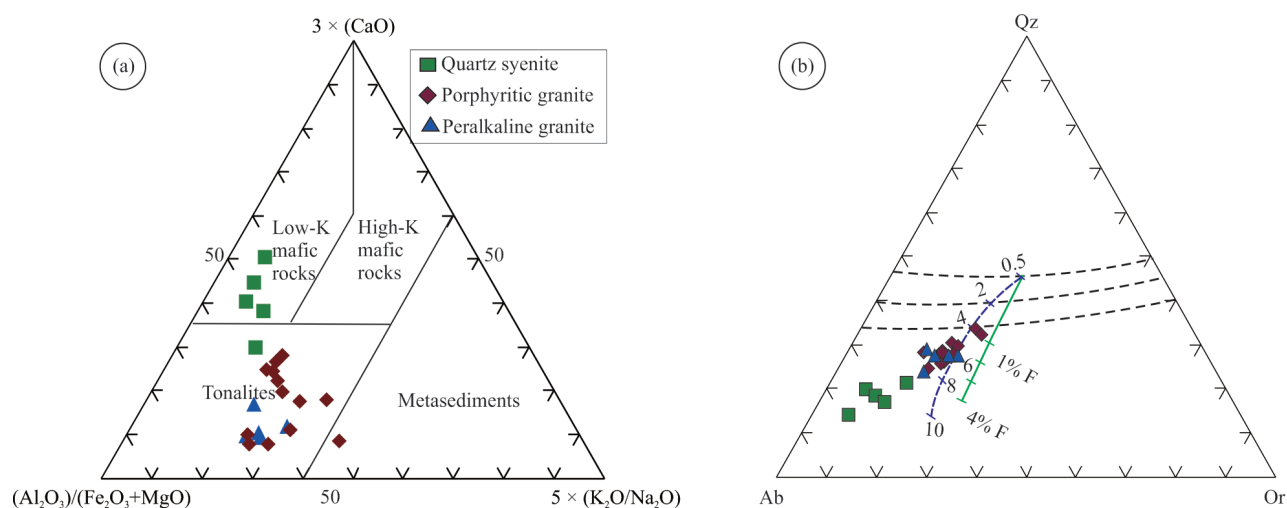
Figure 17. (a) $Al_2O_3/(FeO_t+MgO)$-3CaO-5(K_2O/Na_2O) discrimination diagram for character of source rocks of crustal melts (Laurent et al., 2014); (b) normative composition of Al-Ghurayyah granites plotted in Qz-Ab-Or projection. Dashed lines show the quartz-alkali feldspar cotectics and the trace of the water-saturated minimum melt compositions in the haplogranite system at total pressure ranging from 0.5 to 10 kbar (Holtz et al., 1992; Winkler et al., 1975). Solid green line shows the trace of the minimum melt composition at 1 kbar with excess H_2O and increasing fluorine (F) content up to 4 wt.% F (Manning, 1981).

matic system with fluorine throughout its evolution. Plotting the normative compositions of the Al-Ghurayyah granitoids in the Qz-Ab-Or ternary (Fig. 17b) shows that the samples are too low in normative Qz to be simple H_2O-saturated minimum melts at low pressure. The pressures required to displace the H_2O-saturated minimum melt composition to match the observed rocks are unreasonably high. On the other hand, the addition of 1% to 4% F to the magma drives the cotectic to low enough normative Qz at reasonable upper crustal pressures (Manning, 1981). Increasing water pressure and F content also shift the minimum melt composition towards the albite vertex, but not far enough to match the Al-Ghurayyah rocks, especially the quartz syenite. This implies that there has been alkali exchange with late magmatic or post-magmatic fluids, favoring preservation of albite over K-feldspar.

Although sub-solidus re-equilibration textures and formation of secondary minerals at the expense of K-feldspar and mica occur in the outer margins of Al-Ghurayyah stock, a magmatic origin for the hydrothermal solutions that affected these granites is favored by the following observations: (1) fluorite crystals are found as anhedral to subhedral grains between the rock-forming minerals; (2) concentrations of Nb, Ta, Hf, U and Th increase with progressive fractionation from the early stage (quartz syenite) to the late phase (peralkaline granite); (3) the concentration of pegmatites around the peralkaline granite points to the crystallization of the peralkaline granite as the source of fluids that migrated into and altered the porphyritic granite. Alumina and alkalis liberated from the destruction of feldspars during hydrothermal alteration were transported to the outer and uppermost parts of the stock and drove the formation of secondary muscovite and albite.

The geochemistry of the mineralized silexite veins indicate close affinity and a genetic relationship with the granitoid rock types of the Al-Ghurayyah stock. The end stages of differentiation of the stock produced a residual fluid, distinct from the granitoid minimum melt. This coexisting fluid was en-

riched in SiO_2, volatiles and rare earth elements, and was forcefully emplaced into fractures, faults and shear zones. This fluid had sufficient concentration of elements such as Na, Al, and Fe to crystallize sodic mafic minerals, making it a (perhaps transitional) magmatic fluid distinguishable from the Si- and H_2O-dominant hydrothermal fluids that precipitate common quartz veins. The silexite-forming and pegmatite-forming fluids may have coexisted or may represent different stages in the late evolution of the system. The cataclastic fabric of the silexite possibly resulted from *in situ* fluid loss. Vapor-rich fluid inclusions in quartz phenocrysts suggest that fluids might have been boiled off, resulting in pressure quenching and crystallization of the fine-grained matrix (Jackson and Douch, 1986). Extreme HREE enrichment in the silexite (together with the development of a relative HREE deficit in the peralkaline granite) suggests that no HREE-rich accessory mineral phase was able to sequester these elements at the magmatic stage, leaving them to accumulate in the residual fluid phase.

5.3 Formation of Al-Ghurayyah Granites via Crystal Fractionation

The field studies, mineralogy and geochemistry of the granitoids of the Al-Ghurayyah stock are consistent with evolution through magmatic fractionation from a common parental magma. The good correlations between SiO_2 and most major and trace element concentrations (Figs. 10, 11) as well as the single trends in Rb/Sr *vs.* Sr, Y *vs.* Nb, and Nb *vs.* Rb (Fig. 16) are all consistent with a cogenetic origin by progressive magmatic evolution. The correlation between Eu anomalies and Ba and Sr concentrations in all rock types points to a common cause, namely extreme feldspar fractionation. The effect of alkali feldspar fractionation on the evolution of the studied suite can be investigated using plots of Rb/Ba *vs.* Rb/Sr (Fig. 16d) and Nb *vs.* Ta (Fig. 16e).

The primitive mantle-normalized spider diagrams for the Al-Ghurayyah granitoid samples (Fig. 13) show negative

anomalies for Sr, Eu, Ba, P and Ti. The Sr, Eu and Ba anomalies we have already attributed to feldspar fractionation, whereas the P and Ti anomalies more likely reflect extensive fractionation of apatite and Fe-Ti oxide, respectively. The similar shapes of the spider diagrams and of the REE patterns (Fig. 14) for all phases of the intrusion are consistent with progressive fractional crystallization. Zr/Hf and Nb/Ta ratios are generally invariant during common magmatic processes, but undergo significant variation during magma contamination. The current sample suite is restricted to narrow ranges in both Zr/Hf and Nb/Ta (Fig. 16f) and both ratios are uncorrelated with concentrations of major or trace elements, indicating that contamination played a minor role.

5.4 Evidence of Magmatic *vs*. Metasomatic Effects

Abundant evidence confirms the magmatic origin of the Al-Ghurayyah stock, while also plainly indicating the action of later metasomatic processes. The magmatic features include (1) sharp intrusive contacts of the stock with metamorphic country rock; (2) the coexistence of euhedral to subhedral crystals of primary feldspars, amphibole, columbite and micas; (3) the presence of snowball texture and perthitic exsolution (Müller and Seltmann, 1999; Schwartz, 1992; Pollard, 1989; Vance, 1969), although snowball texture has also been interpreted as metasomatic (Müller and Seltmann, 1999; Beus, 1982); (4) well-developed columbite crystals with normal and oscillatory zoning; (5) anhedral to subhedral grains of fluorite between the constituent minerals; and (6) the gradual increase in REE concentrations from the early phase (quartz syenite) to the late phase (peralkaline granite).

While magmatic features dominate the main phases of the stock, the influence of later hydrothermal fluids becomes more evident in the marginal parts, where extensive replacement by secondary minerals is observed. Hydrothermal fluids appear to have escaped from the peralkaline granite phase and modified the slightly earlier quartz syenite and porphyritic granite phases. Evidence for alteration by these fluids includes: (1) development of pegmatites and quartz-fluorite veins in fractures; (2) partial replacement of microcline crystals by pseudomorphs of secondary albite; (3) overgrowth of secondary albite around primary feldspars and quartz; (4) partial alteration of feldspar crystals to sericite and muscovite; and (5) overgrowth and partial replacement of primary columbite by more Ta-rich columbite and tantalite. It is difficult to explain the concentration of these alteration features in the early phases of the intrusion specifically around the contacts with the late phase of the intrusion if the timing of alteration or source of the fluids were not related to the emplacement and crystallization of the late peralkaline granite phase.

The development of the Nb-Ta oxides in the Al-Ghurayyah system began with crystallization of euhedral to subhedral crystals of primary columbite-(Mn). Experimental studies show that fluxes and melt compositions have strong effects on the solubility of tantalum and niobium oxides (e.g., McNeil et al., 2020; Fiege et al., 2018; van Lichtervelde et al., 2018; Tang et al., 2016). According to Linnen and Keppler (1997), columbite can crystallize from melts that have MnO+FeO contents >0.05 wt.% and Nb concentrations of 70–100 μg/g. The solubility of

rare metal complexes in magmas decreases with decreasing temperature (Chevychelov et al., 2005), so crystallization of primary columbite is significantly more likely in H_2O- and F-rich systems with depression of the solidus to ~600 °C. The presence of well-developed zoning in the columbite crystals and the positive correlation of whole-rock Nb and Ta with SiO_2 (Fig. 12) indicate magmatic enrichment of Ta and Nb. The association of columbite with magmatic micas in the peralkaline granite supports the idea of crystallization of both phases from volatile-rich residual melts at low temperature (van Lichtervelde et al., 2018; Roda et al., 2007).

The primary columbite-(Mn) cores are overgrown and partly replaced by more Ta-rich columbite and tantalite. In principle, such a progression towards increasing Ta/(Ta+Nb) may be explained as a primary magmatic fractionation trend (e. g., Černý et al., 1986), but this would be expected to correlate with systematic increase in Mn/(Mn+Fe) (as seen, e.g., in the Homrit Akarem and Nuweibi intrusions; Abuamarah et al., 2022; Moussa et al., 2021). Other essentially magmatic explanations would include disequilibrium growth limited by slow and differential diffusion of Nb and Ta from the melt to the growing crystal interface, or progressive changes in the equilibrium conditions (Sami et al., 2017). In the Al-Ghurayyah case, the regularly zoned cores are surrounded by Ta-enriched zones without systematic change in Mn/(Mn+Fe) (Fig. 8b) and with common evidence of embayment and resorption of the core. This mineral chemistry and texture pattern is best explained as an overprint due to a late- to post-magmatic, corrosive, supercritical vapor phase (van Lichtervelde et al., 2007). The characteristics of the columbite-tantalite grains (core and rim texture with embayment, enrichment of Ta in the rim, overlap in Mn/(Mn+Fe)) resemble the case described in the Mueilha intrusion, where the case for hydrothermal overprinting is strengthened by association of the tantalite rims with fluorcalciomicrolite and wodginite (Seddik et al., 2020).

6 CONCLUSIONS

(1) The Al-Ghurayyah stock, in the northwest arm of the Arabian Shield, is an example of alkaline felsic magmatism that hosts rare-metal mineralization. It intrudes a Neoproterozoic island arc assemblage and consists of three granitoid varieties (quartz syenite, porphyritic granite and peralkaline granite) as well as veins of pegmatite, silexite and fluorite.

(2) The Al-Ghurayyah granitoids are characterized by highly elevated concentrations of Nb, Ta, Y, Zr, Hf, Th, REE (especially HREE) and Zn.

(3) The accumulation of residual volatile-rich melt and exsolved fluids in the final stages of magmatic evolution produced pegmatite, silexite and quartz-fluorite veins that cut the peripheries of the Al-Ghurayyah stock and promoted alkali metasomatism and recrystallization of Nb-Ta oxides in the early-emplaced granitoid phases.

(4) The Al-Ghurayyah stock is post-collisional A-type granite, derived mainly by fractional crystallization of a crustally-derived parental magma. The geochemical and geological observations are consistent with the lithospheric delamination model for the late Neoproterozoic evolution of the Arabian Shield.

ACKNOWLEDGMENTS

Electronic Supplementary Materials: Supplementary materials (Tables S1–S17) are available in the online version of this article at https://doi.org/10.1007/s12583-022-1708-z.

Conflict of Interest

The authors declare that they have no conflict of interest.

REFERENCES CITED

Abdallah, S. E., Azer, M. K., Al Shammari, A. S., 2020. The Petrological and Geochemical Evolution of Ediacaran Rare-Metal Bearing A-Type Granites from the Jabal Aja Complex, Northern Arabian Shield, Saudi Arabia. *Acta Geologica Sinica* (*English Edition*), 94(3): 743–762 (in Chinese with English Abstract)

Abdel-Karim, A. A. M., El-Shafei, S. A., Azer, M. K., 2021. The Neoproterozoic Ophiolitic Ultramafic Rocks in Eastern Desert of Egypt: Implications for Petrogenesis and Metasomatic Processes. *International Geology Review*, 63(2): 208–232. https://doi.org/10.1080/00206814.2019.1708816

Abuamarah, B. A., 2020. Genesis and Petrology of Postcollisional Rare-Metal-Bearing Granites in the Arabian Shield: A Case Study of Aja Ring Complex, Northern Saudi Arabia. *The Journal of Geology*, 128(2): 131–156. https://doi.org/10.1086/707236

Abuamarah, B. A., Azer, M. K., Asimow, P. D., et al., 2021. Geochemistry and Petrogenesis of Late Ediacaran Rare-Metal Albite Granites of the Arabian-Nubian Shield. *Acta Geologica Sinica-English Edition*, 95(2): 459–480. https://doi.org/10.1111/1755-6724.14379

Abuamarah, B. A., Azer, M. K., Asimow, P. D., et al., 2021. Petrogenesis of the Post-Collisional Rare-Metal-Bearing Ad-Dayheen Granite Intrusion, Central Arabian Shield. *Lithos*, 384/385: 105956. https://doi.org/10.1016/j.lithos.2020.105956

Abuamarah, B. A., Azer, M. K., Seddik, A. M. A., et al., 2022. Magmatic and Post-Magmatic Evolution of Post-Collisional Rare-Metal Bearing Granite: The Neoproterozoic Homrit Akarem Granitic Intrusion, South Eastern Desert of Egypt, Arabian-Nubian Shield. *Geochemistry*, 82(1): 125840. https://doi.org/10.1016/j.chemer.2021.125840

Aleinikoff, J. N., Stoeser, D. B., 1988. Zircon Morphology and U-Pb Geochronology of Seven Metaluminous and Peralkaline Post-Orogenic Granite Complexes of the Arabian Shield, Kingdom of Saudi Arabia (No. 88-604). US Geological Survey

Ali, K. A., Azer, M. K., Gahlan, H. A., et al., 2010. Age Constraints on the Formation and Emplacement of Neoproterozoic Ophiolites along the Allaqi-Heiani Suture, South Eastern Desert of Egypt. *Gondwana Research*, 18(4): 583–595. https://doi.org/10.1016/j.gr.2010.03.002

Ali, K. A., Jeon, H., Andresen, A., et al., 2014. U-Pb Zircon Geochronology and Nd–Hf–O Isotopic Systematics of the Neoproterozoic Hadb Adh Dayheen Ring Complex, Central Arabian Shield, Saudi Arabia. *Lithos*, 206/207: 348–360. https://doi.org/10.1016/j.lithos.2014.07.030

Al-Saleh, A. M., Al-Omari, F. H., 2021. The Qutn Granite, a Hotspot-Related A-Type Granite from the Northeastern Arabian Shield? *Arabian Journal of Geosciences*, 14(9): 1–45. https://doi.org/10.1007/s12517-021-06706-2

Aseri, A. A., 2020. Rare-Metal Alkaline Granite from the Arabian Shield, Saudi Arabia: [Dissertation]. University of Western Ontario, Ontario

Azer, M. K., Stern, R. J., Kimura, J. I., 2010. Origin of a Late Neoproterozoic (605 ± 13 Ma) Intrusive Carbonate–Albitite Complex in Southern Sinai, Egypt. *International Journal of Earth Sciences*, 99(2): 245–267. https://doi.org/10.1007/s00531-008-0385-1

Azer, M. K., Asimow, P. D., Wilde, S. A., 2021. Volcanism during the Post-Accretionary Stage of the Arabian-Nubian Shield. The Geology of the Arabian-Nubian Shield. Springer International Publishing, Cham. https://doi.org/10.1007/978-3-030-72995-0_20

Batchelor, R. A., Bowden, P., 1985. Petrogenetic Interpretation of Granitoid Rock Series Using Multicationic Parameters. *Chemical Geology*, 48(1/2/3/4): 43–55. https://doi.org/10.1016/0009-2541(85)90034-8

Beus, A. A., 1982. Metallogeny of Precambrian Rare-Metal Granitoids. *Revista Brasileira de Geociencias*, 12: 410–413

Bonin, B., 2007. A-Type Granites and Related Rocks: Evolution of a Concept, Problems and Prospects. *Lithos*, 97(1/2): 1–29. https://doi.org/10.1016/j.lithos.2006.12.007

Černý, P., Goad, B. E., Hawthorne, F., et al., 1986. Fractionation Trends of the Nb- and Ta-Bearing Oxide Minerals in the Greer Lake Pegmatitic Granite and Its Pegmatite Aureole, Southeastern Manitoba. *American Mineralogist*, 71(3/4): 501–517

Chevychelov, V. Y., Zaraisky, G. P., Borisovskii, S. E., et al., 2005. Effect of Melt Composition and Temperature on the Partitioning of Ta, Nb, Mn, and F between Granitic (Alkaline) Melt and Fluorine-Bearing Aqueous Fluid: Fractionation of Ta and Nb and Conditions of ore Formation in Rare-Metal Granites. *Petrology*, 13(4): 305

Clark, M. D., 1987. Explanatory Notes to the Geologic Map of the Al Bada Quadrangle, Sheet 28A, Kingdom of Saudi Arabia, 46

de la Roche, H., Leterrier, J., Grandclaude, P., et al., 1980. A Classification of Volcanic and Plutonic Rocks Using R_1R_2-Diagram and Major-Element Analyses—Its Relationships with Current Nomenclature. *Chemical Geology*, 29(1/2/3/4): 183–210. https://doi.org/10.1016/0009-2541(80)90020-0

Deer, W. A., Howie, R. A., Zussman, J., 1992. An Introduction to the Rock Forming Minerals. Second Edition, Longman Scientific and Technical, London, 696

Drysdall, A. R., Douch, C. J., 1986. NBTHZR Mineralization in Microgranite—Microsyenite at Jabal Tawlah, Midyan Region, Kingdom of Saudi Arabia. *Journal of African Earth Sciences*, 4: 275–288. https://doi.org/10.1016/s0899-5362(86)80089-6

Drysdall, A. R., Jackson, N. J., Ramsay, C. R., 1985. Rare-Element Mineralization Related to Alkali Granites of the Hijaz Region, with Representative Geochemical Data. Open file Report, DGMR-OF-05-12, Jiddah, Kingdom of Saudi Arabia, 40

Drysdall, A. R., Jackson, N. J., Ramsay, C. R., et al., 1984. Rare Element Mineralization Related to Precambrian Alkali Granites in the Arabian Shield. *Economic Geology*, 79(6): 1366–1377. https://doi.org/10.2113/gsecongeo.79.6.1366

du Bray, E. A., 1986. Specialized Granitoids in the Southeastern Arabian Shield—Case History of a Regional Assessment. *Journal of African Earth Sciences* (*1983*), 4: 169–176. https://doi.org/10.1016/s0899-5362(86)80077-x

Eby, G. N., 1990. The A-Type Granitoids: A Review of Their Occurrence and Chemical Characteristics and Speculations on Their Petrogenesis. *Lithos*, 26(1/2): 115–134. https://doi.org/10.1016/0024-4937(90)9004

3-z

Eby, G. N., 1992. Chemical Subdivision of the A-Type Granitoids: Petrogenetic and Tectonic Implications. *Geology*, 20(7): 641–644. https://doi.org/10.1130/0091-7613(1992)0200641:csotat>2.3.co;2

Elliott, J. E., Al-Yazidi, S., Al-Eissa, H., et al., 1999. Exploration of the Ghurayyah Radioactive Granite, Kingdom of Saudi Arabia. Saudi Geological Survey Technical Report (OpenFile Report 2001-7)

Evensen, N. M., Hamilton, P. J., O'Nions, R. K., 1978. Rare-Earth Abundances in Chondritic Meteorites. *Geochimica et Cosmochimica Acta*, 42(8): 1199–1212. https://doi.org/10.1016/0016-7037(78)90114-x

Eyal, M., Litvinovsky, B., Jahn, B. M., et al., 2010. Origin and Evolution of Post-Collisional Magmatism: Coeval Neoproterozoic Calc-Alkaline and Alkaline Suites of the Sinai Peninsula. *Chemical Geology*, 269(3/4): 153–179. https://doi.org/10.1016/j.chemgeo.2009.09.010

Farahat, E. S., Azer, M. K., 2011. Post-Collisional Magmatism in the Northern Arabian-Nubian Shield: The Geotectonic Evolution of the Alkaline Suite at Gebel Tarbush Area, South Sinai, Egypt. *Geochemistry*, 71(3): 247–266. https://doi.org/10.1016/j.chemer.2011.06.003

Fiege, A., Simon, A., Linsler, S. A., et al., 2018. Experimental Constraints on the Effect of Phosphorous and Boron on Nb and Ta Ore Formation. *Ore Geology Reviews*, 94: 383–395. https://doi.org/10.1016/j.oregeorev.2018.02.007

Frost, B. R., Barnes, C. G., Collins, W. J., et al., 2001. A Geochemical Classification for Granitic Rocks. *Journal of Petrology*, 42(11): 2033–2048. https://doi.org/10.1093/petrology/42.11.2033

Gahlan, H. A., Asimow, P. D., Azer, M. K., et al., 2021. Geochemistry and Mineralogy of the Jebel Aja Igneous Intrusion and the Associated Exotic Pegmatites, Arabian Shield, Saudi Arabia. *Lithos*, 400/401: 106395. https://doi.org/10.1016/j.lithos.2021.106395

Gahlan, H. A., Azer, M. K., Al-Hashim, M. H., et al., 2022. Highly Evolved Rare-Metal Bearing Granite Overprinted by Alkali Metasomatism in the Arabian Shield: A Case Study from the Jabal Tawlah Granites. *Journal of African Earth Sciences*, 192: 104556. https://doi.org/10.1016/j.jafrearsci.2022.104556

Hanson, G. N., 1978. The Application of Trace Elements to the Petrogenesis of Igneous Rocks of Granitic Composition. *Earth and Planetary Science Letters*, 38(1): 26–43. https://doi.org/10.1016/0012-821x(78)90124-3

Harris, N. B. W., Pearce, J. A., Tindle, A. G., 1986. Geochemical Characteristics of Collision-Zone Magmatism. *Geological Society, London, Special Publications*, 19(1): 67–81. https://doi.org/10.1144/gsl.sp.1986.019.01.04

Hawthorne, F. C., Oberti, R., Harlow, G. E., et al., 2012. Nomenclature of the Amphibole Supergroup. *American Mineralogist*, 97(11/12): 2031–2048. https://doi.org/10.2138/am.2012.4276

Hedge, C. E., 1984. Precambrian Geochronology of Part of Northwestern Saudi Arabia. Saudi Arabian Deputy Ministry for Mineral Resources: Jiddah, Saudi Arabia. USGS-OF-84-381

Holtz, F., Behrens, H., Dingwell, D. B., et al., 1992. Water Solubility in Aluminosilicate Melts of Haplogranite Composition at 2 Kbar. *Chemical Geology*, 96(3/4): 289–302. https://doi.org/10.1016/0009-2541(92)90060-i

Jackson, N. J., 1986. Mineralization Associated with Felsic Plutonic Rocks in the Arabian Shield. *Journal of African Earth Sciences* (*1983*), 4: 213–227. https://doi.org/10.1016/s0899-5362(86)80083-5

Jackson, N. J., Douch, C. J., 1986. Jabal Hamra REE-Mineralized Silexite, Hijaz Region, Kingdom of Saudi Arabia. *Journal of African Earth Sciences* (*1983*), 4: 269–274. https://doi.org/10.1016/s0899-5362(86)80088-4

Johnson, P. R., 2006. Explanatory Notes to the Map of Proterozoic Geology of Western Saudi Arabia. Saudi Geological Survey Technical Report SGS-TR-2006-4, 62

Johnson, P. R., Andresen, A., Collins, A. S., et al., 2011. Late Cryogenian–Ediacaran History of the Arabian–Nubian Shield: A Review of Depositional, Plutonic, Structural, and Tectonic Events in the Closing Stages of the Northern East African Orogen. *Journal of African Earth Sciences*, 61(3): 167–232. https://doi.org/10.1016/j.jafrearsci.2011.07.003

Laurent, O., Martin, H., Moyen, J. F., et al., 2014. The Diversity and Evolution of Late-Archean Granitoids: Evidence for the Onset of "Modern-Style" Plate Tectonics between 3.0 and 2.5 Ga. *Lithos*, 205: 208–235. https://doi.org/10.1016/j.lithos.2014.06.012

Liégeois, J. P., Black, R., 1987. Alkaline Magmatism Subsequent to Collision in the Pan-African Belt of the Adrar des Iforas (Mali). *Geological Society, London, Special Publications*, 30(1): 381–401. https://doi.org/10.1144/gsl.sp.1987.030.01.18

Liégeois, J. P., Navez, J., Hertogen, J., et al., 1998. Contrasting Origin of Post-Collisional High-K Calc-Alkaline and Shoshonitic Versus Alkaline and Peralkaline Granitoids. The Use of Sliding Normalization. *Lithos*, 45(1/2/3/4): 1–28. https://doi.org/10.1016/s0024-4937(98)00023-1

Linnen, R. L., Keppler, H., 1997. Columbite Solubility in Granitic Melts: Consequences for the Enrichment and Fractionation of Nb and Ta in the Earth's Crust. *Contributions to Mineralogy and Petrology*, 128(2): 213–227. https://doi.org/10.1007/s004100050304

London, D., 1992. The Application of Experimental Petrology to the Genesis and Crystallization of Granitic Pegmatites. *Canadian Mineralogist*, 30(3): 499–540 (in Chinese with English Abstract)

Maniar, P. D., Piccoli, P. M., 1989. Tectonic Discrimination of Granitoids. *Geological Society of America Bulletin*, 101(5): 635–643. https://doi.org/10.1130/0016-7606(1989)1010635:tdog>2.3.co;2

Manning, D. A. C., 1981. The Effect of Fluorine on Liquidus Phase Relationships in the System Qz-Ab-or with Excess Water at 1 Kb. *Contributions to Mineralogy and Petrology*, 76(2): 206–215. https://doi.org/10.1007/bf00371960

McKay, G. A., 2018. Partitioning of Rare Earth Elements between Major Silicate Minerals and Basaltic Melts. *Reviews in Mineralogy and Geochemistry*, 21: 45–78

McNeil, A. G., Linnen, R. L., Flemming, R. L., 2020. Solubility of Wodginite, Titanowodginite, Microlite, Pyrochlore, Columbite-(Mn) and Tantalite-(Mn) in Flux-Rich Haplogranitic Melts between 700° and 850 °C and 200 MPa. *Lithos*, 352/353: 105239. https://doi.org/10.1016/j.lithos.2019.105239

Miller, C., Stoddard, E. F., Bradfish, L. J., et al., 1981. Composition of Plutonic Muscovite; Genetic Implications. *Canadian Mineralogist*, 19(1): 25–34

Moghazi, A. K M., Iaccheri, L. M., Bakhsh, R. A., et al., 2015. Sources of Rare-Metal-Bearing A-Type Granites from Jabel Sayed Complex, Northern Arabian Shield, Saudi Arabia. *Journal of Asian Earth Sciences*, 107: 244–258. https://doi.org/10.1016/j.jseaes.2015.04.042

Moghazi, A. M., Harbi, H. M., Ali, K. A., 2011. Geochemistry of the Late Neoproterozoic Hadb Adh Dayheen Ring Complex, Central Arabian Shield: Implications for the Origin of Rare-Metal-Bearing Post-Orogenic A-Type Granites. *Journal of Asian Earth Sciences*, 42(6): 1324–1340. https://doi.org/10.1016/j.jseaes.2011.07.018

Moussa, H. E., Asimow, P. D., Azer, M. K., et al., 2021. Magmatic and Hydrothermal Evolution of Highly-Fractionated Rare-Metal Granites at Gabal Nuweibi, Eastern Desert, Egypt. *Lithos*, 400/401: 106405. https://doi.org/10.1016/j.lithos.2021.106405

Muller, A., Seltmann, R., 1999. The Genetic Significance of Snowball Quartz in High Fractionated tin Granites of the Krušne Hory/ Erzgebirge. *Mineral Deposits: Processes to Processing*, 1: 409–412

Pfänder, J. A., Münker, C., Stracke, A., et al., 2007. Nb/Ta and Zr/Hf in Ocean Island Basalts—Implications for Crust-Mantle Differentiation and the Fate of Niobium. *Earth and Planetary Science Letters*, 254(1/2): 158–172. https://doi.org/10.1016/j.epsl.2006.11.027

Pollard, P. J., 1989. Geologic Characteristics and Genetic Problems Associated with the Development of Granite-Hosted Deposits of Tantalum and Niobium. Lanthanides, Tantalum and Niobium. Springer, Berlin, Heidelberg, 240–256. https://doi.org/10.1007/978-3-642-87262-4_9

Putnis, A., 2009. Mineral Replacement Reactions. *Reviews in Mineralogy and Geochemistry*, 70(1): 87–124. https://doi.org/10.2138/rmg.2009.70.3

Ramsay, C. R., 1982. Geology and Mineral Resource Potential of Pan-African Granitoid Rocks, Northern Midyan Region, Saudi Arabia. Saudi Arabian Deputy Ministry for Petroleum and Mineral Resources, Open-File Report DGMR-OF-02-11

Ramsay, C. R., 1986. Specialized Felsic Plutonic Rocks of the Arabian Shield and Their Precursors. *Journal of African Earth Sciences*, 4: 153–168. https://doi.org/10.1016/s0899-5362(86)80076-8

Ramsay, C. R., Odell, J., Drysdall, A. R., 1986. Felsic Plutonic Rocks of the Midyan Region, Kingdom of Saudi Arabia—II. Pilot Study in Chemical Classification of Arabian Granitoids. *Journal of African Earth Sciences*, 4: 79–85. https://doi.org/10.1016/s0899-5362(86)800 69-0

Roda, E., Keller, P., Pesquera, A., et al., 2007. Micas of the Muscovite – Lepidolite Series from Karibib Pegmatites, Namibia. *Mineralogical Magazine*, 71(1): 41–62. https://doi.org/10.1180/minmag.2007.07 1.1.41

Sami, M., Ntaflos, T., Farahat, E. S., et al., 2017. Mineralogical, Geochemical and Sr-Nd Isotopes Characteristics of Fluorite-Bearing Granites in the Northern Arabian-Nubian Shield, Egypt: Constraints on Petrogenesis and Evolution of Their Associated Rare Metal Mineralization. *Ore Geology Reviews*, 88: 1–22. https://doi.org/10.1016/j.oregeorev.2017.04.015

Schwartz, M. O., 1992. Geochemical Criteria for Distinguishing Magmatic and Metasomatic Albite-Enrichment in Granitoids—Examples from the Ta-Li Granite Yichun (China) and the Sn-W Deposit Tikus (Indonesia). *Mineralium Deposita*, 27(2): 101–108. https://doi.org/10.1007/bf00197092.

Seddik, A. M. A., Darwish, M. H., Azer, M. K., et al., 2020. Assessment of Magmatic Versus Post-Magmatic Processes in the Mueilha Rare-Metal Granite, Eastern Desert of Egypt, Arabian-Nubian Shield. *Lithos*, 366/367: 105542. https://doi.org/10.1016/j.lithos.2020.105542

Stepanov, A.S., Hermann, J., 2013. Fractionation of Nb and Ta by Biotite and Phengite: Implications for the "Missing Nb Paradox". *Geology*, 41(3): 303–306

Stern, R. J., 1994. Arc Assembly and Continental Collision in the Neoproterozoic East African Orogen: Implications for the Consolidation of Gondwanaland. *Annual Review of Earth and Planetary Sciences*, 22: 319–351. https://doi.org/10.1146/annurev.ea.22.050194.001535

Stern, R. J., Ali, K. A., Liegeois, J. P., et al., 2010. Distribution and Significance of Pre-Neoproterozoic Zircons in Juvenile Neoproterozoic Igneous Rocks of the Arabian-Nubian Shield. *American Journal of Science*, 310(9): 791–811. https://doi.org/10.2475/09.2010.02

Stern, R. J., Johnson, P., 2010. Continental Lithosphere of the Arabian Plate: A Geologic, Petrologic, and Geophysical Synthesis. *Earth-Science Reviews*, 101(1/2): 29–67. https://doi.org/10.1016/j.earscirev.2010.01.002

Sun, S. S., McDonough, W. F., 1989. Chemical and Isotopic Systematics of Oceanic Basalts: Implications for Mantle Composition and Processes. *Geological Society, London, Special Publications*, 42(1): 313–345. https://doi.org/10.1144/gsl.sp.1989.042.01.19

Sylvester, P. J., 1989. Post-Collisional Alkaline Granites. *The Journal of Geology*, 97(3): 261–280. https://doi.org/10.1086/629302

Tang, Y., Zhang, H., Rao, B., 2016. The Effect of Phosphorus on Manganocolumbite and Mangaotantalite Solubility in Peralkaline to Peraluminous Granitic Melts. *American Mineralogist*, 101(2): 415–422. https://doi.org/10.2138/am-2016-5424

Turner, S. P., Foden, J. D., Morrison, R. S., 1992. Derivation of some A-Type Magmas by Fractionation of Basaltic Magma: An Example from the Padthaway Ridge, South Australia. *Lithos*, 28(2): 151–179. https://doi.org/10.1016/0024-4937(92)90029-x

van Lichtervelde, M., Holtz, F., Melcher, F., 2018. The Effect of Disequilibrium Crystallization on Nb-Ta Fractionation in Pegmatites: Constraints from Crystallization Experiments of Tantalite-Tapiolite. *American Mineralogist*, 103(9): 1401–1416. https://doi.org/10.2138/am-2018-6441

Van Lichtervelde, M., Salvi, S., Beziat, D., et al., 2007. Textural Features and Chemical Evolution in Tantalum Oxides: Magmatic Versus Hydrothermal Origins for Ta Mineralization in the Tanco Lower Pegmatite, Manitoba, Canada. *Economic Geology*, 102(2): 257–276. https://doi.org/10.2113/gsecongeo.102.2.257

Vance, J. A., 1969. On Synneusis. *Contributions to Mineralogy and Petrology*, 24(1): 7–29. https://doi.org/10.1007/bf00398750

Vonopartis, L. C., Kinnaird, J. A., Nex, P. A. M., et al., 2021. African A-Type Granites: A Geochemical Review on Metallogenic Potential. *Lithos*, 396/397: 106229. https://doi.org/10.1016/j.lithos.2021.106229

Wedepohl, K. H., 1995. The Composition of the Continental Crust. *Geochimica et Cosmochimica Acta*, 59(7): 1217–1232. https://doi.org/10.1016/0016-7037(95)00038-2

Whalen, J. B., Currie, K. L., Chappell, B. W., 1987. A-Type Granites: Geochemical Characteristics, Discrimination and Petrogenesis. *Contributions to Mineralogy and Petrology*, 95(4): 407–419. https://doi.org/10.1007/bf00402202

Winkler, H. G. F., Boese, M., Marcopoulos, T., 1975. Low Temperature Granite Melts. Neues Jahrbuchfür Mineralogie. *Monatshefte*, 6: 245–268

Winter, J. D., 2014. Principles of Igneous and Metamorphic Petrology (Vol. 2). Pearson Education, Harlow

Winter, J. D., 2001. An Introduction to Igneous and Metamorphic Petrology. Prentice Hall Inc. Upper Saddle River, 697